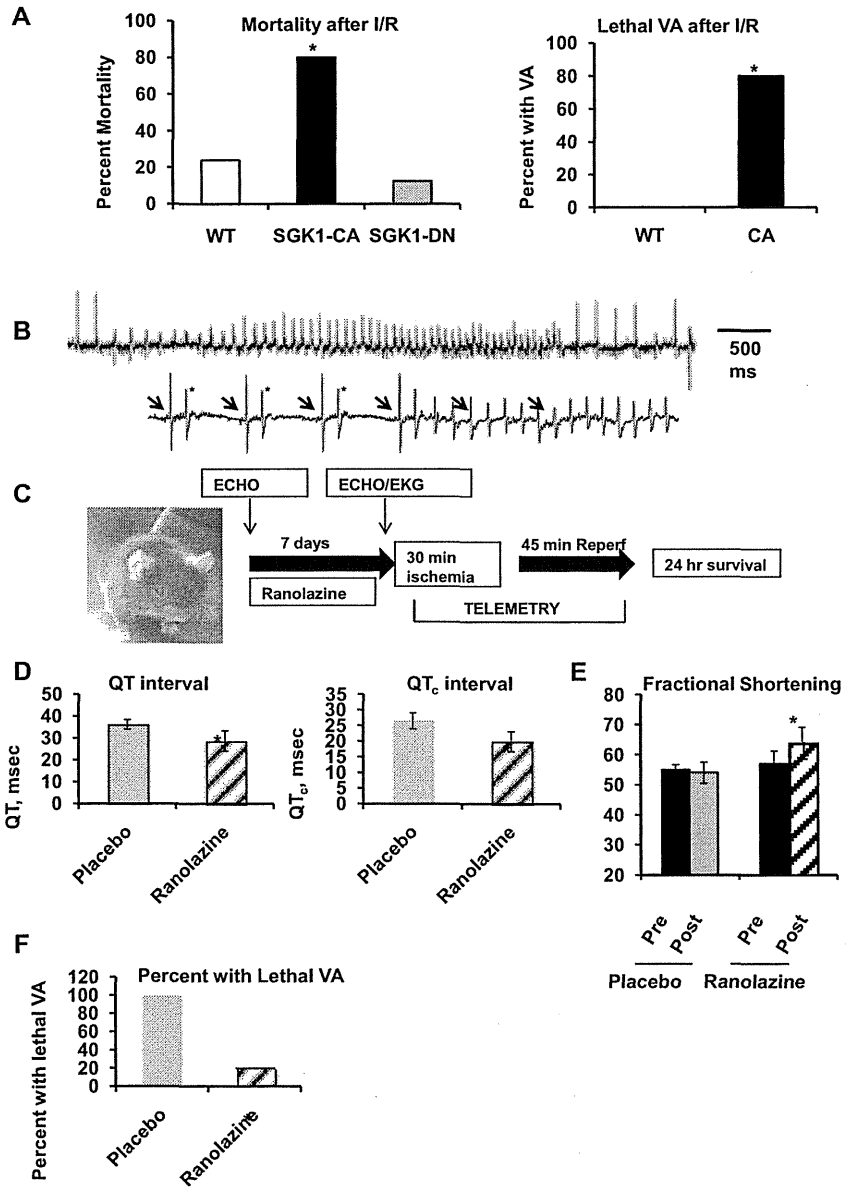

Figure 6. Increased susceptibility to ventricular arrhythmias and cardiac dysfunction in SGK1-CA mice can be reversed by ranolazine. **A,** Mortality is increased in SGK1-CA mice after ischemia-reperfusion (I/R: 30 minutes LAD ligation/24 hours reperfusion). **Left,** mortality in SGK1-CA (8/10), WT (7/29), and SGK1-DN (2/16) mice, $*P<0.005$ by Z test of proportions. **Right,** Telemetry demonstrated that SGK1-CA mice develop lethal ventricular arrhythmias (VAs) (4/5) after I/R that were not seen in WT mice (0/4) $*P=0.02$ by Z test. **B,** Representative tracings of VA in SGK1-CA mice during reperfusion. Lower tracing shows ventricular bigeminy (asterisks) before onset of ventricular tachycardia with AV dissociation (arrows denote p waves). **C,** Schema for in vivo ranolazine experiments. **D,** Ranolazine decreases QT and QT_c intervals in SGK1-CA mice in comparison with placebo ($*P<0.05$ by unequal variance t test or Mann-Whitney test). **E,** Fractional shortening was better in SGK1-CA mice after 7 days of ranolazine treatment than in mice treated with placebo ($*P<0.05$ by 2-way repeated-measures ANOVA). In paired t tests, mice treated with ranolazine showed a nonsignificant trend toward improved fractional shortening ($P=0.055$), whereas there was no change in placebo-treated mice ($P=0.59$). **F,** Incidence of lethal VA after I/R was decreased in ranolazine-treated SGK1-CA mice in comparison with placebo ($*P<0.05$ by Z test of proportions). WT indicates wild type; SGK1, serum- and glucocorticoid-regulated kinase-1; DN, dominant negative; CA, constitutively active; LAD, left anterior descending artery; and ANOVA, analysis of variance.

Thus, chronic SGK1 activation and TAC-HF increase trafficking of Nav1.5 to the HM fraction, whereas SGK1 inhibition blocks this response to TAC, suggesting SGK1 is both necessary and sufficient for these changes.

The increase in HM Nav1.5 would be expected to increase Na^+-channel surface availability. To test this directly, we used biotin to label surface-exposed proteins in neonatal rat ventricular myocytes expressing either SGK1-CA or green fluorescent protein, and selectively collected labeled surface proteins with an avidin-coupled column. As controls, the transmembrane protein, Glut 4, was labeled and recovered robustly from the surface of both green fluorescent protein- and SGK1-CA–expressing neonatal rat ventricular myocytes, while GSK3β, a cytoplasmic protein, was not (Figure 7A). SGK1-CA expression increased the amount of biotin-labeled Nav1.5 in neonatal rat ventricular myocytes in comparison with green fluorescent protein–transduced cells (Figure 7A). These data are consistent with the hypothesis that SGK1 activation increases the amount of Nav1.5 available at the cell surface.

Activation of SGK1 in renal tubular cells leads to phosphorylation of the ubiquitin ligase, Nedd4-2,[30,31] and decreased binding of the phospho-Nedd4-2 to the PY motif of E_{NaC}, which increases surface expression and channel activity of E_{NaC}.[32] Nav1.5 has also been shown to bind to Nedd4-2 via a conserved PY motif in its C-terminal tail,[33] and in a heterologous expression system, decreased binding of Nedd4-2 to Nav1.5 leads to increased Nav1.5 membrane expression.[34] We therefore examined if altered Nedd4-2 binding plays a role in Nav1.5 trafficking in response to TAC or SGK1 activation in vivo. Nedd4-2 coimmunoprecipitated with the Na channel in sham-operated WT hearts, and there was a marked decrease in Nedd4-2 binding to Na channels in TAC-HF and SGK1-CA hearts (Figure 7B). In contrast,

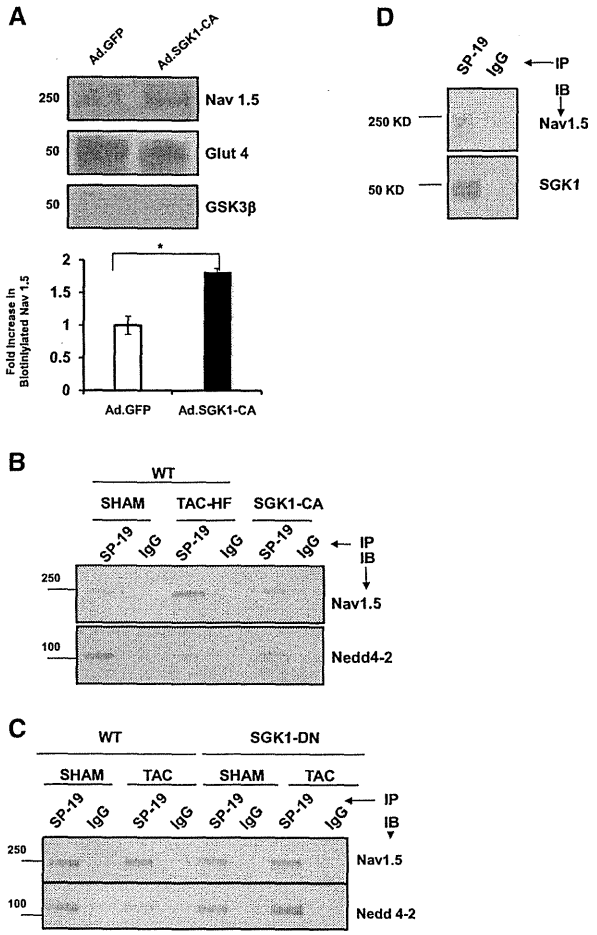

Figure 7. SGK1 activation is necessary and sufficient for alterations in cardiac sodium channel seen in failing hearts. **A**, Cardiomyocytes were infected with either Ad.SGK1-CA or Ad.GFP, and biotin labeled to tag surface (eg, Nav1.5, Glut4) but not cytoplasmic proteins (eg, GSK3β). Biotin-labeled proteins were captured by using an avidin column and subjected to immunoblotting. SGK1-CA expression increased surface expression of Nav1.5. *P<0.05, n=3 independent experiments. **B**, Total heart lysates from WT (sham-operated), TAC-HF, or unoperated SGK1-CA mice were immunoprecipitated with a pan-Na^+-channel antibody (SP-19). Immunoblotting with antibodies to Nav1.5 or Nedd4-2 showed a decrease in Nedd4-2 binding in TAC-HF and SGK1-CA hearts. **C**, Cardiac lysates from SGK1-DN transgenic or WT mice subjected to TAC or sham operation were immunoprecipitated with SP-19 and immunoblotted with the antibody-specific Nav1.5 or Nedd4-2 (**bottom**). The decrease in Nedd4-2 binding to Nav1.5 seen in failing WT hearts is completely prevented in SGK1-DN hearts after TAC. **D**, SGK1 directly associates with Nav1.5. Sodium channel was immunoprecipitated from heart lysates by using SP-19 or control IgG antibody-coupled columns and subjected to immunoblotting as labeled. Figures are representative of 3 independent experiments. WT indicates wild type; SGK1, serum- and glucocorticoid-regulated kinase-1; DN, dominant negative; CA, constitutively active; TAC, transverse aortic constriction; and TAC-HF, TAC-induced heart failure.

SGK1-DN preserved Nedd4-2 binding to Na channels after TAC (Figure 7C). Thus, SGK1 activation appears both necessary and sufficient for the alterations in Nedd4-2 binding to Nav1.5 seen after TAC- HF.

It seems likely that the observed alterations in Nedd4-2 binding and surface-available Na channel contribute to overall increases in I_{Na} but not the observed changes in channel gating and kinetics. To investigate other possible contributing mechanisms, we next examined whether SGK1 physically interacts with Nav1.5 protein. Immunoprecipitation experiments demonstrated that endogenous SGK1 protein binds the Na channel (Figure 7D). Because isoform-specific Na channel antibodies for immunoprecipitation are not available, it is possible that SGK1 binds not only Nav1.5, but also less abundant channel isoforms present in the heart. This physical association raised the possibility that SGK1 could phosphorylate Nav1.5. To begin to explore this possibility, we determined the SGK1 consensus target sequence by using a peptide library.[35] The preferred phosphorylation target sequence for SGK1 is similar to that for Akt (RKRRnS/T) but differs in the secondary amino acids (online-only Data Supplement Figure IXC). Using the newly defined target motif in ScanSite, we identified 2 consensus sites in SCN5a (S483 and S664, both in the DI-II linker, which have been previously noted[11]) and an additional novel but weaker consensus site (S1590) in the D4/S3 region (online-only Data Supplement Figure IXD).

Overall, our data support the model that SGK1 is both necessary and sufficient for changes seen in Na-channel–Nedd4-2 binding and trafficking in TAC-HF. In addition, SGK1 directly associates with the sodium channel, which harbors multiple consensus target sequences for SGK1 phosphorylation. Cumulatively, these biochemical changes are likely to account for the electrophysiological alterations observed in SGK1-CA cardiomyocytes and mice. Determining the specific functional contributions of these protein–protein interactions, and the putative SGK1 phosphorylation sites, as well, will be of interest for future studies.

Discussion

Heart failure and the ventricular arrhythmias that can accompany it are growing causes of morbidity and mortality around the world.[36] Acute activation of proximal phosphatidylinositol 3-kinase signaling has beneficial effects on cardiomyocyte survival and function[4,5,37] but is paradoxically increased in heart failure and diabetes,[7] raising the possibility that chronic activation of these initially compensatory pathways may become maladaptive. In this context, we investigated the role of SGK1, a serine-threonine kinase that we had previously shown is activated early in pressure overload and acutely promotes cardiomyocyte survival.[5] We found that SGK1 phosphorylation is also increased in animal models of chronic heart failure and human dilated cardiomyopathy. In contrast, SGK1 was not altered in exercise-induced physiological hypertrophy.

TG mice with constitutive cardiac activation of SGK1 spontaneously developed several hallmarks of adverse ventricular remodeling including systolic and diastolic dysfunction, as well as susceptibility to ventricular arrhythmias. The proarrhythmic effects of SGK1 activation were linked to biochemical and functional changes in the cardiac sodium channel that culminated in action potential prolongation and after-depolarizations, as well as an increase in I_{NaL}. APD prolongation and after-depolarizations were completely normalized by treatment with ranolazine at doses that block late

but not peak I_{Na}. Finally, SGK1-CA mice treated with ranolazine in vivo not only showed decreased ECG abnormalities and susceptibility to ventricular arrhythmias, but also had better cardiac function, suggesting that altered sodium flux, specifically increased I_{NaL}, is an important contributor to both the electric and mechanical phenotypes seen with chronic SGK1 activation in the heart. Consistent with this hypothesis, human SCN5a mutations can cause not only arrhythmia, but also cardiomyopathy.[22,38] However, it seems likely that other SGK1 targets also contribute to cardiac dysfunction and fibrosis. The genetic models described in this work should provide useful platforms for identification of such pathways and dissecting their functional contributions to the phenotypes observed.

We also found that SGK1 activation led to biochemical changes in the sodium channel that recapitulated changes seen in TAC-induced heart failure and included reduced association with the ubiquitin ligase, Nedd4-2, and altered channel trafficking resulting in an increase of surface-available Nav1.5. Conversely, inhibition of SGK1 in the SGK1-DN mice blocked the biochemical changes in Nav1.5 after TAC-HF, supporting the specificity of these findings and suggesting SGK1 is also necessary for at least some aspects of electric remodeling. SGK1 bound Nav1.5, and peptide mapping identified several candidate SGK1 targets in the sodium channel. Intriguingly, one of these is in a region important in channel inactivation gating[22] and adjacent to a site mutated (D1595H in the Domain IV/S3 region) in a cardiomyopathy syndrome associated with arrhythmias.[22,38] Testing the functional role of these putative phosphorylation sites will be of interest for future studies.

Taken together, the current study underscores the importance of SGK1 in both cardiac dysfunction and arrhythmia. Other kinases are also important modulators of Nav1.5, including protein kinase A,[39] protein kinase C,[40] and calcium calmodulin-dependent kinase II,[41,42] and, thus, the inhibition SGK1 alone may not fully protect against these phenotypes. Nevertheless, our genetic data suggest that inhibition of SGK1 warrants further investigation as a therapeutic target in these settings, in particular, given the success of therapeutically targeting kinases on other settings.

Acknowledgments

We thank Dr Ling Li for expert technical support and Dr Serafima Zaltsman for managing the mouse colonies.

Sources of Funding

This research was supported by a Leducq Foundation Network of Research Excellence (to Dr Rosenzweig) and the National Institutes of Health (grants R01HL094677 and R21HL104370 to Dr Rosenzweig, KO8HL089319 to Dr Das, and R01HL050411 to Dr Tomaselli). Dr Rosenzweig also gratefully acknowledges support from Judith and David Ganz. He is a principal faculty member of the Harvard Stem Cell Institute and an Associate Member of the Broad Institute.

Disclosures

Dr Das is a trainee of the Clinical Investigators Training Program: BIDMC–Harvard/MIT HST, in collaboration with Pfizer, Inc and Merck & Co.

References

1. Undrovinas AI, Maltsev VA, Kyle JW, Silverman N, Sabbah HN. Gating of the late Na^+ channel in normal and failing human myocardium. *J Mol Cell Cardiol.* 2002;34:1477–1489.
2. Cesario DA, Brar R, Shivkumar K. Alterations in ion channel physiology in diabetic cardiomyopathy. *Endocrinol Metab Clin North Am.* 2006;35: 601–610, ix–x.
3. Matsui T, Li L, del Monte F, Fukui Y, Franke TF, Hajjar RJ, Rosenzweig A. Adenoviral gene transfer of activated phosphatidylinositol 3′-kinase and Akt inhibits apoptosis of hypoxic cardiomyocytes in vitro. *Circulation.* 1999;100:2373–2379.
4. Matsui T, Tao J, del Monte F, Lee K-H, Li L, Picard M, Force TL, Franke TF, Hajjar RJ, Rosenzweig A. Akt activation preserves cardiac function and prevents injury after transient cardiac ischemia in vivo. *Circulation.* 2001;104:330–335.
5. Aoyama T, Matsui T, Novikov M, Park J, Hemmings B, Rosenzweig A. Serum and glucocorticoid-responsive kinase-1 regulates cardiomyocyte survival and hypertrophic response. *Circulation.* 2005;111:1652–1659.
6. Haq S, Choukroun G, Lim H, Tymitz KM, del Monte FF, Gwathmey J, Grazette L, Michael A, Hajjar R, Force T, Molkentin JD. Differential activation of signal transduction pathways in human hearts with hypertrophy versus advanced heart failure. *Circulation.* 2001;103:670–677.
7. Cook SA, Varela-Carver A, Mongillo M, Kleinert C, Khan MT, Leccisotti L, Strickland N, Matsui T, Das S, Rosenzweig A, Punjabi P, Camici PG. Abnormal myocardial insulin signalling in type 2 diabetes and left-ventricular dysfunction. *Eur Heart J.* 2010;31:100–111.
8. Park J, Leong ML, Buse P, Maiyar AC, Firestone GL, Hemmings BA. Serum and glucocorticoid-inducible kinase (SGK) is a target of the PI 3-kinase-stimulated signaling pathway. *EMBO J.* 1999;18:3024–3033.
9. Webster MK, Goya L, Ge Y, Maiyar AC, Firestone GL. Characterization of sgk, a novel member of the serine/threonine protein kinase gene family which is transcriptionally induced by glucocorticoids and serum. *Mol Cell Biol.* 1993;13:2031–2040.
10. Wulff P, Vallon V, Huang DY, Volkl H, Yu F, Richter K, Jansen M, Schlunz M, Klingel K, Loffing J, Kauselmann G, Bosl MR, Lang F, Kuhl D. Impaired renal Na(+) retention in the sgk1-knockout mouse. *J Clin Invest.* 2002;110:1263–1268.
11. Boehmer C, Wilhelm V, Palmada M, Wallisch S, Henke G, Brinkmeier H, Cohen P, Pieske B, Lang F. Serum and glucocorticoid inducible kinases in the regulation of the cardiac sodium channel SCN5A. *Cardiovasc Res.* 2003;57:1079–1084.
12. Matsui T, Li L, Wu JC, Cook SA, Nagoshi T, Picard MH, Liao R, Rosenzweig A. Phenotypic spectrum caused by transgenic overexpression of activated Akt in the heart. *J Biol Chem.* 2002;277:22896–22901.
13. Arany Z, Novikov M, Chin S, Ma Y, Rosenzweig A, Spiegelman BM. Transverse aortic constriction leads to accelerated heart failure in mice lacking PPAR-gamma coactivator 1alpha. *Proc Natl Acad Sci U S A.* 2006;103:10086–10091.
14. Berul CI, Aronovitz MJ, Wang PJ, Mendelsohn ME. In vivo cardiac electrophysiology studies in the mouse. *Circulation.* 1996;94:2641–2648.
15. Morissette MR, Cook SA, Foo S, McKoy G, Ashida N, Novikov M, Scherrer-Crosbie M, Li L, Matsui T, Brooks G, Rosenzweig A. Myostatin regulates cardiomyocyte growth through modulation of Akt signaling. *Circ Res.* 2006;99:15–24.
16. Song KS, Li S, Okamoto T, Quilliam LA, Sargiacomo M, Lisanti MP. Co-purification and direct interaction of ras with caveolin, an integral membrane protein of caveolae microdomains. Detergent-free purification of caveolae microdomains. *J Biol Chem.* 1996;271:9690–9697.
17. Kaab S, Nuss HB, Chiamvimonvat N, O'Rourke B, Pak PH, Kass DA, Marban E, Tomaselli GF. Ionic mechanism of action potential prolongation in ventricular myocytes from dogs with pacing-induced heart failure. *Circ Res.* 1996;78:262–273.
18. Aiba T, Hesketh GG, Barth AS, Liu T, Daya S, Chakir K, Dimaano VL, Abraham TP, O'Rourke B, Akar FG, Kass DA, Tomaselli GF. Electrophysiological consequences of dyssynchronous heart failure and its restoration by resynchronization therapy. *Circulation.* 2009;119:1220–1230.
19. Subramaniam A, Jones WK, Gulick J, Wert S, Neumann J, Robbins J. Tissue-specific regulation of the alpha-myosin heavy chain gene promoter in transgenic mice. *J Biol Chem.* 1991;266:24613–24620.
20. Brunet A, Park J, Tran H, Hu LS, Hemmings BA, Greenberg ME. Protein kinase SGK mediates survival signals by phosphorylating the forkhead transcription factor FKHRL1 (FOXO3a). *Mol Cell Biol.* 2001;21: 952–965.
21. Abriel H, Cabo C, Wehrens XH, Rivolta I, Motoike HK, Memmi M, Napolitano C, Priori SG, Kass RS. Novel arrhythmogenic mechanism

revealed by a long-QT syndrome mutation in the cardiac Na(+) channel. *Circ Res.* 2001;88:740–745.
22. Nguyen TP, Wang DW, Rhodes TH, George AL Jr. Divergent biophysical defects caused by mutant sodium channels in dilated cardiomyopathy with arrhythmia. *Circ Res.* 2008;102:364–371.
23. Chandra R, Starmer CF, Grant AO. Multiple effects of KPQ deletion mutation on gating of human cardiac Na+ channels expressed in mammalian cells. *Am J Physiol.* 1998;274:H1643–H1654.
24. Dumaine R, Wang Q, Keating MT, Hartmann HA, Schwartz PJ, Brown AM, Kirsch GE. Multiple mechanisms of Na+ channel–linked long-QT syndrome. *Circ Res.* 1996;78:916–924.
25. Valdivia CR, Chu WW, Pu J, Foell JD, Haworth RA, Wolff MR, Kamp TJ, Makielski JC. Increased late sodium current in myocytes from a canine heart failure model and from failing human heart. *J Mol Cell Cardiol.* 2005;38:475–483.
26. Fredj S, Sampson KJ, Liu H, Kass RS. Molecular basis of ranolazine block of LQT-3 mutant sodium channels: evidence for site of action. *Br J Pharmacol.* 2006;148:16–24.
27. Kloner RA, Dow JS, Bhandari A. First direct comparison of the late sodium current blocker ranolazine to established antiarrhythmic agents in an ischemia/reperfusion model. *J Cardiovasc Pharmacol Ther.* 2011;16:192–196.
28. Belardinelli L, Shryock JC, Fraser H. Inhibition of the late sodium current as a potential cardioprotective principle: effects of the late sodium current inhibitor ranolazine. *Heart.* 2006;92(suppl 4):iv6–iv14.
29. Yarbrough TL, Lu T, Lee HC, Shibata EF. Localization of cardiac sodium channels in caveolin-rich membrane domains: regulation of sodium current amplitude. *Circ Res.* 2002;90:443–449.
30. Staub O, Verrey F. Impact of nedd4 proteins and serum and glucocorticoid-induced kinases on epithelial Na+ transport in the distal nephron. *J Am Soc Nephrol.* 2005;16:3167–3174.
31. Snyder PM, Olson DR, Thomas BC. Serum and glucocorticoid-regulated kinase modulates Nedd4–2-mediated inhibition of the epithelial Na+ channel. *J Biol Chem.* 2002;277:5–8.
32. Diakov A, Korbmacher C. A novel pathway of epithelial sodium channel activation involves a serum- and glucocorticoid-inducible kinase consensus motif in the C terminus of the channel's alpha-subunit. *J Biol Chem.* 2004;279:38134–38142.
33. Abriel H, Kamynina E, Horisberger JD, Staub O. Regulation of the cardiac voltage-gated Na+ channel (H1) by the ubiquitin-protein ligase Nedd4. *FEBS Lett.* 2000;466:377–380.
34. van Bemmelen MX, Rougier JS, Gavillet B, Apotheloz F, Daidie D, Tateyama M, Rivolta I, Thomas MA, Kass RS, Staub O, Abriel H. Cardiac voltage-gated sodium channel Nav1.5 is regulated by Nedd4–2 mediated ubiquitination. *Circ Res.* 2004;95:284–291.
35. Hutti JE, Jarrell ET, Chang JD, Abbott DW, Storz P, Toker A, Cantley LC, Turk BE. A rapid method for determining protein kinase phosphorylation specificity. *Nat Methods.* 2004;1:27–29.
36. Redfield MM. Heart failure–an epidemic of uncertain proportions. *N Engl J Med.* 2002;347:1442–1444.
37. Nagoshi T, Matsui T, Aoyama T, Leri A, Anversa P, Li L, Ogawa W, del Monte F, Gwathmey JK, Grazette L, Hemmings BA, Kass DA, Champion HC, Rosenzweig A. PI3K rescues the detrimental effects of chronic Akt activation in the heart during ischemia/reperfusion injury. *J Clin Invest.* 2005;115:2128–2138.
38. Olson TM, Michels VV, Ballew JD, Reyna SP, Karst ML, Herron KJ, Horton SC, Rodeheffer RJ, Anderson JL. Sodium channel mutations and susceptibility to heart failure and atrial fibrillation. *JAMA.* 2005;293:447–454.
39. Zhou J, Yi J, Hu N, George AL Jr, Murray KT. Activation of protein kinase a modulates trafficking of the human cardiac sodium channel in xenopus oocytes. *Circ Res.* 2000;87:33–38.
40. West JW, Numann R, Murphy BJ, Scheuer T, Catterall WA. A phosphorylation site in the Na+ channel required for modulation by protein kinase C. *Science.* 1991;254:866–868.
41. Wagner S, Dybkova N, Rasenack EC, Jacobshagen C, Fabritz L, Kirchhof P, Maier SK, Zhang T, Hasenfuss G, Brown JH, Bers DM, Maier LS. Ca2+/calmodulin-dependent protein kinase ii regulates cardiac Na+ channels. *J Clin Invest.* 2006;116:3127–3138.
42. Maltsev VA, Reznikov V, Undrovinas NA, Sabbah HN, Undrovinas A. Modulation of late sodium current by Ca2+, calmodulin, and CaMKII in normal and failing dog cardiomyocytes: similarities and differences. *Am J Physiol Heart Circ Physiol.* 2008;294:H1597–H1608.

CLINICAL PERSPECTIVE

Patients with heart failure have an increased risk of ventricular arrhythmias and sudden cardiac death. Heart failure is associated with changes in the electrical properties of the heart that form the triggers and substrate for ventricular arrhythmias. Available antiarrhythmic drugs have not shown any clinical benefit in patients with heart failure and have significant proarrhythmic side effects. To gain a better understanding of mechanisms that underlie the electrical changes in heart failure, we focused on the serum- and glucocorticoid-regulated kinase-1 (SGK1), a component of the cardiac phosphatidylinositol 3-kinase signaling pathway that is activated in heart failure. Our results demonstrated that activation of SGK1 in the heart increased mortality, cardiac dysfunction, and ventricular arrhythmias. The proarrhythmic effects of SGK1 were linked to biochemical and functional changes in the cardiac sodium channel and could be reversed by treatment with ranolazine, a blocker of the late sodium current. Conversely, inhibition of SGK1 in the heart protected against fibrosis, heart failure, and sodium channel alterations after hemodynamic stress. Our studies highlight the importance of sodium flux in the pathogenesis of arrhythmia in heart failure and raise the possibility that drugs that block the late sodium current could be useful in this setting. Moreover, these results identify SGK1 as a novel kinase target for treatment of both arrhythmia and cardiac dysfunction. The potential clinical importance of this observation is underscored by the therapeutic success of kinase inhibitors in other disease processes.

Subcellular Structures and Function of Myocytes Impaired During Heart Failure Are Restored by Cardiac Resynchronization Therapy

Frank B. Sachse,* Natalia S. Torres,* Eleonora Savio-Galimberti, Takeshi Aiba, David A. Kass, Gordon F. Tomaselli, John H. Bridge

Rationale: **Cardiac resynchronization therapy (CRT) is an established treatment for patients with chronic heart failure. However, CRT-associated structural and functional remodeling at cellular and subcellular levels is only partly understood.**

Objective: **To investigate the effects of CRT on subcellular structures and protein distributions associated with excitation-contraction coupling of ventricular cardiomyocytes.**

Methods and Results: **Our studies revealed remodeling of the transverse tubular system (t-system) and the spatial association of ryanodine receptor (RyR) clusters in a canine model of dyssynchronous heart failure (DHF). We did not find this remodeling in a synchronous heart failure model based on atrial tachypacing. Remodeling in DHF ranged from minor alterations in anterior left ventricular myocytes to nearly complete loss of the t-system and dissociation of RyRs from sarcolemmal structures in lateral cells. After CRT, we found a remarkable and almost complete reverse remodeling of these structures despite persistent left ventricular dysfunction. Studies of whole-cell Ca^{2+} transients showed that the structural remodeling and restoration were accompanied with remodeling and restoration of Ca^{2+} signaling.**

Conclusions: **DHF is associated with regional remodeling of the t-system. Myocytes undergo substantial structural and functional restoration after only 3 weeks of CRT. The finding suggests that t-system status can provide an early marker of the success of this therapy. The results could also guide us to an understanding of the loss and remodeling of proteins associated with the t-system. The steep relationship between free Ca^{2+} and contraction suggests that some restoration of Ca^{2+} release units will have a disproportionately large effect on contractility. (*Circ Res.* 2012;110:588-597.)**

Key Words: dyssynchronous heart failure ■ cardiac resynchronization therapy ■ cellular remodeling ■ excitation-contraction coupling ■ transverse tubular system

Heart failure (HF) is associated with a grim prognosis. For patients with moderate or severe symptoms annual mortality can be as high as 30–60%, despite pharmacological treatment.[1,2] Initial remodeling of structure, metabolism, and electrophysiology probably compensates for defects produced by HF. These changes are ultimately maladaptive and may be associated with progression of the HF phenotype, arrhythmias, and sudden cardiac death. It has been estimated that ≈40% of patients with HF have conduction delays associated with dyssynchronous electric activation and mechanical contraction of the left ventricle. This dyssynchronous activation is an independent predictor of both total mortality and sudden cardiac death in HF patients.[3] Simultaneous pacing of the right and left ventricles, a procedure called cardiac resynchronization therapy (CRT), is a major advance in the treatment of patients with moderate to severe chronic HF (New York Heart Association class III or IV). CRT alleviates the marked regional heterogeneity of ventricular function and mechanical loading. CRT reduces symptoms and mortality in about 70% of patients who exhibit resynchronization of mechanical contraction.[1,2] However, exactly what causes improvements in heart function resulting

Original received September 24, 2011; revision received January 5, 2012; accepted January 9, 2012. In December 2011, the average time from submission to first decision for all original research papers submitted to *Circulation Research* was 14.29 days.

From the Nora Eccles Harrison Cardiovascular Research and Training Institute (F.B.S., N.S.T., E.S.-G., J.H.B.) and the Department of Bioengineering (F.B.S.), University of Utah, Salt Lake City, UT; and the Division of Cardiology (T.A., D.A.K., G.F.T.) and the Department of Biomedical Engineering (D.A.K.), Johns Hopkins University School of Medicine, Baltimore, MD.

*These authors contributed equally to this paper.

The online-only Data Supplement is available with this article at http://circres.ahajournals.org/lookup/suppl/doi:10.1161/CIRCRESAHA.111.257428/-/DC1.

Correspondence to Dr. Frank B. Sachse, University of Utah, Nora Eccles Harrison Cardiovascular Research and Training Institute, 95 South 2000 East, Salt Lake City, UT 84112-5000. E-mail fs@cvrti.utah.edu

Circulation Research **is available at http://circres.ahajournals.org** **DOI: 10.1161/CIRCRESAHA.111.257428**

from CRT and what subcellular mechanism(s) underlie this therapy are only poorly understood. It is even less clear why a significant number of patients do not benefit from CRT.

There is an extensive literature addressing the subcellular structural alterations in HF,[4–8] with some variability in structural and functional remodeling in differing forms of experimental and human HF. Some of the more consistent cellular features of HF are prolongation of action potential duration, impaired contraction, and impaired Ca^{2+} homeostasis with heterogeneous alterations in the amplitudes and kinetics of Ca^{2+} transients. The functional remodeling is associated with alterations in the mRNA and protein expression and posttranslational modification of a number of proteins involved in Ca^{2+} signaling underlying excitation-contraction (EC) coupling.[9–11]

We used a canine pacing tachycardia model to study consequences and mechanisms of dyssynchronous heart failure (DHF) and CRT. In this model of DHF produced by left bundle-branch ablation and rapid right atrial pacing, we characterized the electrical and hemodynamic remodeling as well as changes in intracellular Ca^{2+} transients and a variety of channel and transporter proteins.[11,12] We demonstrated that DHF causes dyssynchronous anterior-septal and lateral strain[13] as well as dyssynchronous septal and lateral strain rates.[14] Recently, we reported DHF associated changes in the regional cardiac transcriptome primarily of the left anterior wall.[15] Some of these alterations are to some extent reversed by CRT, which also reduces regional heterogeneity of gene expression and dyssynchrony of strains and strain rates.

Remarkably, little is known about the reorganization of subcellular structures and protein distributions associated with EC coupling during DHF and after CRT. The transverse tubular system (t-system) is a crucially important subcellular structure for efficient EC coupling.[16–18] In ventricular cardiomyocytes, this system consists of membrane invaginations, which are essential for rapid transmission of electric signals from the outer sarcolemma into the cell interior. The t-system extends in close proximity to the sarcoplasmic reticulum, which allows their membrane proteins to form multimolecular complexes including L-type Ca^{2+} channels in the sarcolemma and ryanodine receptors (RyRs) in the membrane of the sarcoplasmic reticulum apposed to the t-tubules. These complexes are called couplons.[19,20] Alterations of the t-system and the associated proteins unquestionably underlie many of the defects produced by HF.[8,18] Three-dimensional microscopic imaging and image analysis are essential to fully understand the nature of structural remodeling of the t-system, as this cannot be assessed in 2-dimensional images.[21] In particular, the changes in density and orientation of subcellular structures can only be appreciated in 3D reconstructions. In addition, 3D imaging allows one to obtain a detailed understanding of any restoration of such structures as a result of CRT. We investigated for the first time an initial remodeling of t-tubules and RyR clusters as a result of DHF and a remarkable and almost complete reverse remodeling of these structures after CRT despite the persistence of left ventricular dysfunction. Studies of whole-cell Ca^{2+} transients revealed that both structural remodeling and restoration were accompanied by remodeling and restoration of Ca^{2+} signaling. Our findings of substantial restoration of structure and function after only 3 weeks of CRT suggest that the t-system can provide an early marker of the success of this therapy.

Non-standard Abbreviations and Acronyms	
CRT	cardiac resynchronization therapy
DHF	dyssynchronous heart failure
RyR	ryanodine receptor
TTP	time to peak
t-system	transverse tubular system
WGA	wheat germ agglutinin

Methods

HF and CRT Models

The animal models of DHF and CRT have been described previously.[13,22,23] In brief, adult male mongrel dogs were used as control and DHF and CRT models. DHF animals underwent right atrial pacing (200 bpm) for 6 weeks after radiofrequency ablation of the left bundle-branch. CRT animals underwent left bundle-branch radiofrequency ablation and 3 weeks of right atrial pacing followed by 3 weeks of resynchronization by biventricular pacing at the same pacing rate. We also studied animals without left bundle-branch ablation who underwent 6 weeks of right atrial pacing also at 200 bpm (A6) to generate a model of synchronous HF. Hemodynamic data were measured that characterize control, DHF, CRT, and A6 animals. The data confirm that the paced animals in all groups develop HF and with the most depressed maximal upstroke of the left ventricular blood pressure (dP/dt_{max}) in the DHF animals (Online Table I). Myocytes were isolated enzymatically from the anterior and lateral mid myocardium of the left ventricle. We used cells from 10 control, 8 A6, 7 DHF, and 11 CRT animals (Online Table II).

Labeling and Imaging of Sarcolemma and RyRs

Cells were labeled using wheat germ agglutinin (WGA) conjugated to Alexa Fluo-555 and monoclonal anti-RyR2 antibody with a secondary goat anti-mouse IgG (H+L) antibody attached to Alexa Fluor 488 (further detail in the online-only Data Supplement). Three-dimensional image stacks of labeled cells immersed in glycerol were acquired, using a confocal microscope (LSM 5 Live Duo, Carl Zeiss, Jena, Germany) equipped with a 63× oil immersion lens (Numeric aperture, 1.4). The imaging configuration is shown in Online Figure I. Details regarding our imaging protocol are provided in the online-only Data Supplement. Online Table II presents the number of cells and animals that were applied for reconstruction, analysis, and visualization.

Reconstruction of Sarcolemma and RyR Clusters

The preprocessing of confocal microscopic images is described in the online-only Data Supplement. The sarcolemma was detected by thresholding of the WGA image stacks followed by median filtering.[24] The threshold was calculated from image statistics and set to mode+SD. Image stacks were segmented in outer sarcolemmal, t-system, and intracellular and extracellular regions by morphological operators.[25] Euclidean distance maps were calculated from the sarcolemmal regions. RyR clusters were extracted by maxima search and region-growing methods from the image stacks of

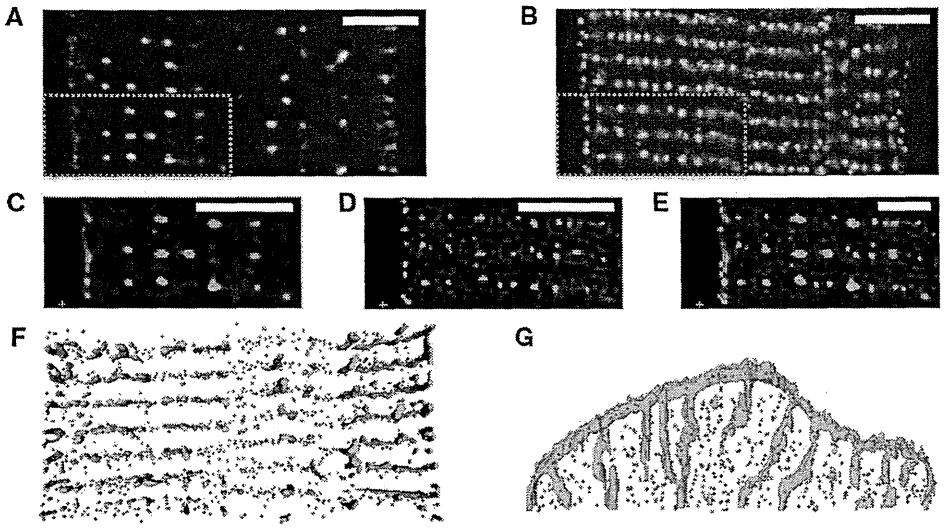

Figure 1. Imaging and reconstruction of cardiac myocytes from lateral left ventricle of normal canine. Confocal microscopic images of **A**, sarcolemma labeled with WGA, and **B**, antibody labeled RyRs. **C** and **D**, Deconvolved images zooming into marked regions in **A** and **B**. WGA is shown in blue, RyRs in red. **E**, Overlay of images showing regular arrangement of t-system and RyR clusters. Three-dimensional reconstruction of WGA distribution and centers of RyR clusters, **F**, horizontal section shown from above; **G**, vertical section (shown laterally). Scale bar: 5 μm.

anti-RyR2 antibody–labeled myocytes. The threshold was set to mode+4 SD. Centers of RyR clusters were identified by the centers of mass of segmented regions. Density (number of clusters per unit volume) and distances between RyR cluster centers were calculated to quantify the spatial distribution of RyR clusters. Distances of RyR clusters to the sarcolemma (including t-system) were determined from probing the distance maps at cluster centers.

Measurement and Analysis of Ca^{2+} Transients

Whole-cell Ca^{2+} transients were measured and analyzed as described by us previously.[11,12,25] Myocytes from the lateral left ventricle were incubated with the Ca^{2+} indicator Indo-1-AM (Molecular Probes, Eugene, OR). Measurements were performed at 37°C, using 1-Hz field stimulation. The indicator was excited at a wavelength of 365 nm. Emitted light at 405 and 495 nm was collected with an inverted microscope (Ellipse TE2001, Nikon) equipped with an image/fluorescence system (MyoCam, IonOptix, MA). Signals were digitized and stored for subsequent analysis. The ratio of fluorescence at 405 and 495 nm (F405/485) was calculated after subtraction of cellular autofluorescence. The decay of the Ca^{2+} transients (tau) was determined by fitting a single exponential to the ratioed fluorescence. Each experimental group included cells from at least 3 animals.

Statistical Analysis

All statistical analyses of the image stacks were performed with Matlab 7.9. Density of RyR clusters, distances of RyR clusters to the sarcolemma, and RyR-nearest-neighbor distances are presented as mean±SD. Significance of was determined by a 2-tailed Student *t* test, using a 5% significance level.

Results

Spatial Organization of T-Tubules and RyRs in Canine Ventricular Myocytes

We first studied control canine cells isolated from both the anterior and lateral walls of the left ventricle. The sarcolemma, including t-tubules, and RyRs were labeled with WGA conjugate and monoclonal antibodies, respectively. We obtained image stacks of myocyte segments (Online Figure I). Figure 1 displays the arrangement of t-tubules and RyR clusters in a segment of a myocyte isolated from the lateral wall of the left ventricle. T-tubules are arrayed regularly and appear in the vicinity of the z-disks as transverse rows (Figure 1A and 1C) in the *y*-axis. RyRs are clearly registered in the *y*-axis (Figure 1B and 1D), similarly to the t-tubules. This becomes clear in the overlay of WGA and RyR images (Figure 1E), where many RyR clusters appear colocalized with t-tubules and presumably form couplons. The image indicates that a significant number of RyR clusters are not associated with t-tubules. This is clearer in Figure 1F and 1G, which display 3D reconstructions of RyRs and t-tubules in the myocyte segment. The t-tubules and RyRs tend to form sheets in the vicinity of the z disks. Reconstructions of t-tubules and RyR clusters in control anterior cells displayed similar features (Online Figure II).

A detailed analysis of the 3D reconstructions from anterior and lateral ventricular cells (Figure 2) revealed distances between centers of RyR clusters and the sarcolemma that are similar in both cell types (0.44±0.51 μm and 0.41±0.49 μm, respectively). Also, a nearest-neighbor analysis of RyRs did not show significant differences in anterior and lateral cells (0.62±0.37 μm versus 0.63±0.38 μm). We used Fourier analysis to characterize the spatial distribution of t-tubules and RyRs in 3D. The analysis was constrained to spatial frequencies corresponding to spatial periodicities of z-disks (2.0±0.5 μm). Intensity histograms were calculated in sectors with an opening angle of 10° (Online Figure III). Maxima in the Fourier histogram from RyRs and WGA images appear at the sectors to 90° (Figure 2C and 2D), which indicates regular arrangement of the labeled structures along the *y*-axis. A local maximum in the WGA Fourier histogram at 0–10° indicates regular arrangement of the t-tubules along the *x*-axis. The Fourier histograms are almost identical in both anterior and lateral cells.

Characterization of T-Tubules and RyRs in A6 Myocytes

We analyzed A6 cells using the same methods as applied to control cells. Reconstructions of t-tubules and RyR clusters in A6 cells displayed features similar to control cells (Online Figure IV). Differences of the RyR cluster-sarcolemma distance

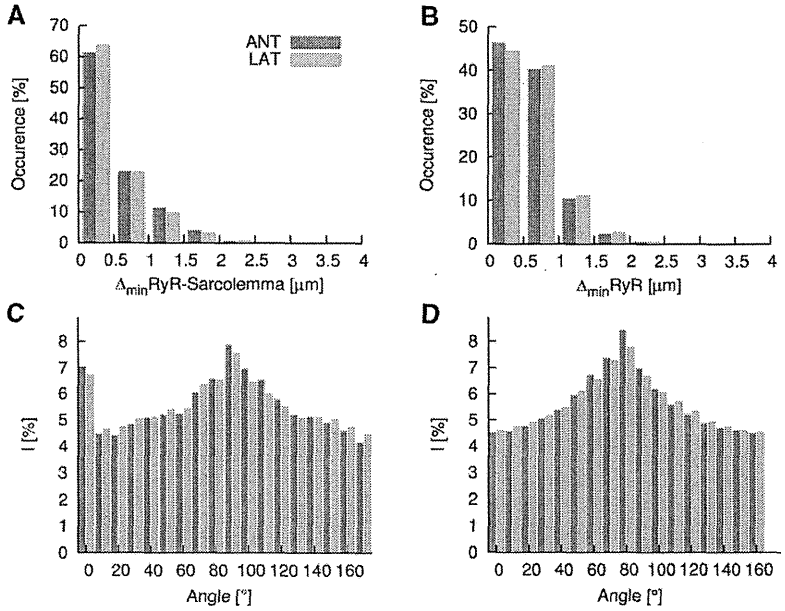

Figure 2. Quantitative characterization of cardiac myocytes from lateral (LAT) and anterior (ANT) left ventricle of normal canine. A, Histogram of distances between RyR clusters and the closest sarcolemma. The majority of RyR clusters are in close proximity of the sarcolemma. **B,** Histogram of distances of RyR clusters to their nearest neighbor. Fourier intensities of **C,** WGA, and **D,** RyR-labeled image stacks. Both intensity distributions exhibit a maxima close to 90°, corresponding to *y*-axis components of the spectrum.

between anterior and lateral cells were not significant (0.45±0.49 μm and 0.41±0.47 μm, respectively). Similarly, differences of the nearest neighbor distance of RyR clusters in both cell types were not significant (0.64±0.40 μm and 0.64±0.40 μm, respectively). Control and A6 lateral cells exhibited insignificant differences for the RyR cluster density (0.44±0.08/μm^3 versus 0.50±0.06/μm^3).

Remodeling of T-Tubules and RyR Distributions in Myocytes After DHF

We studied the alterations in distribution of t-tubules and RyRs in isolated left ventricular cells taken from dog hearts 6 weeks after left bundle-branch ablation and rapid atrial pacing. Using this protocol, the hearts had exhibited severe systolic dysfunction and the animals were in HF. We examined cells from both the lateral and anterior ventricular walls. Anterior cells from DHF ventricles did not show striking alterations when they were visually compared with control cells. This is apparent in the deconvolved images and reconstructions displayed in Figure 3A. However, in lateral ventricular cells, it is immediately apparent that the t-tubular system was dramatically remodeled. A striking example is presented in Figure 3B. The t-system is sparse centrally. T-tubules in the cell periphery exhibit longitudinal components. Furthermore,

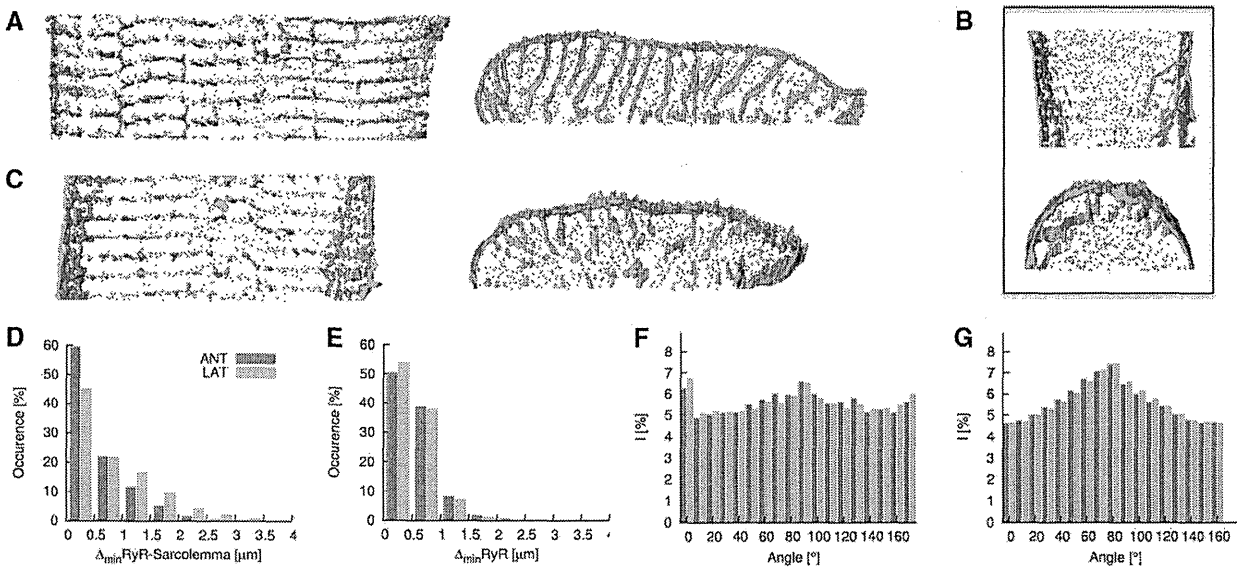

Figure 3. Characterization of cardiac myocytes from left ventricle of DHF canine. Deconvolved confocal microscopic images and 3D reconstructions of segment of **A,** anterior, and **B** and **C,** lateral cells. Lateral cells exhibit structural alterations, in particular, sparseness and increased longitudinal components of the t-system, and reduced alignment of RyR clusters. Histogram of **D,** distances between RyR clusters and the closest sarcolemma, and **E,** distances of RyR clusters to their nearest neighbor. Fourier intensities of **F,** WGA, and **G,** RyR-labeled image stacks.

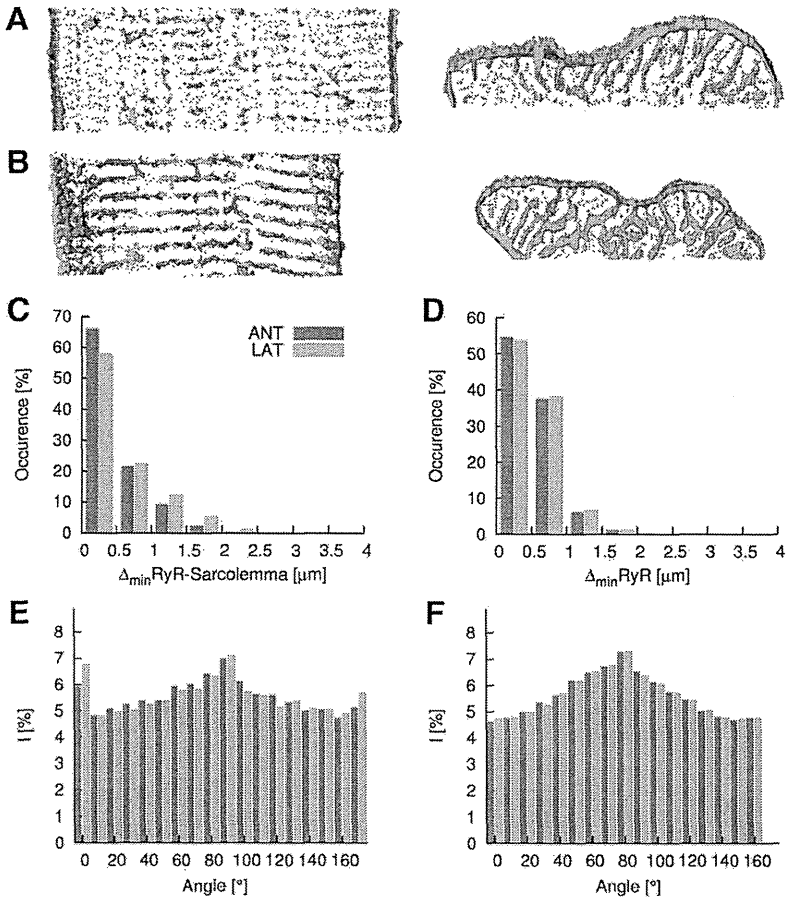

Figure 4. Characterization of cardiac myocytes from left ventricle of canine after CRT. Deconvolved confocal microscopic images and 3D reconstructions of segment of **A**, anterior, and **B**, lateral cells. Histograms of **C**, distances between RyR clusters and the closest sarcolemma, and **D**, distances of RyR clusters to their nearest neighbor. Fourier intensities of **E**, WGA, and **F**, RyR-labeled image stacks.

the cell shows a loss of alignment of RyRs. A less extreme case of t-tubule remodeling is shown in Figure 3C. These consequences of DHF are apparent in the 2D optical slices, the 3D reconstructions viewed from above the myocyte, and along the major axis of the myocyte. An effect of t-system remodeling in DHF is that the majority of RyRs are not associated with sarcolemmal structures. In comparison to control and A6, distances between RyR clusters and the nearest sarcolemma increased significantly in DHF lateral cells (0.66±0.72 μm) but not in anterior cells (0.48±0.58 μm) (Figure 3D). The nearest-neighbor distance of RyR clusters showed little change between anterior and lateral cells (0.63±0.38 μm and 0.59±0.35 μm, respectively) and when compared with control and A6 cells (Figure 3E versus Figure 2B and Online Figure IV, D).

Again we used Fourier analysis to characterize the spatial distribution of t-tubules and RyRs from anterior and lateral DHF cells (Figure 3F and 3G). Maxima in the Fourier histogram from WGA images appear for sectors at 0–10° and 90–100° for both cell types (Figure 3F). In comparison to normal cells (Figure 2C), the maximum indicating regular arrangement of the t-tubules along the *y*-axis is reduced. The Fourier histograms from RyR images indicate that the arrangement of RyR clusters is similar in normal and DHF cells of both types (Figure 3G versus Figure 2D). This type of analysis allowed us to describe changes in the distribution of RyRs and t-tubules in both DHF cells and after these cells have been subject to CRT.

Partial Restoration of T-Tubules and RyR Distributions After CRT

We investigated the spatial distributions of t-tubules and RyRs in myocytes after they had been paced to induce DHF for 3 weeks and were then subject to rapid pacing CRT for 3 weeks. The effects on these structures were not distributed uniformly throughout the heart. First, because DHF produces relatively small effects in anterior cells, it is perhaps not surprising to find that there was little effect of CRT on these cell types. This is clear from Figure 4A. However, there was a remarkable reverse structural remodeling of t-tubules after CRT in lateral cells. This is obvious from visual inspection of Figure 4B and is particularly apparent in the 3D reconstruction of the cell segment viewed from the z-direction (middle panel) and y-direction (right panel). RyR–nearest sarcolemma distances were 0.40±0.50 μm and 0.48±0.57 μm for anterior and lateral cells, respectively. Our measurements of RyR–nearest sarcolemma distances (Figure 4C versus Figure 3D) indicate that the t-system is not completely restored, but the remodeling is striking, with t-tubules assuming a more normal distribution, that is, resembling controls. Some longitudinal components of the t-system remain, but these are reduced. CRT did not affect the nearest-neighbor distance of RyR clusters in anterior and lateral cells (0.59±0.35 μm and 0.61±0.36 μm, respectively) (Figure 4D), which was also not altered in DHF in both cell types.

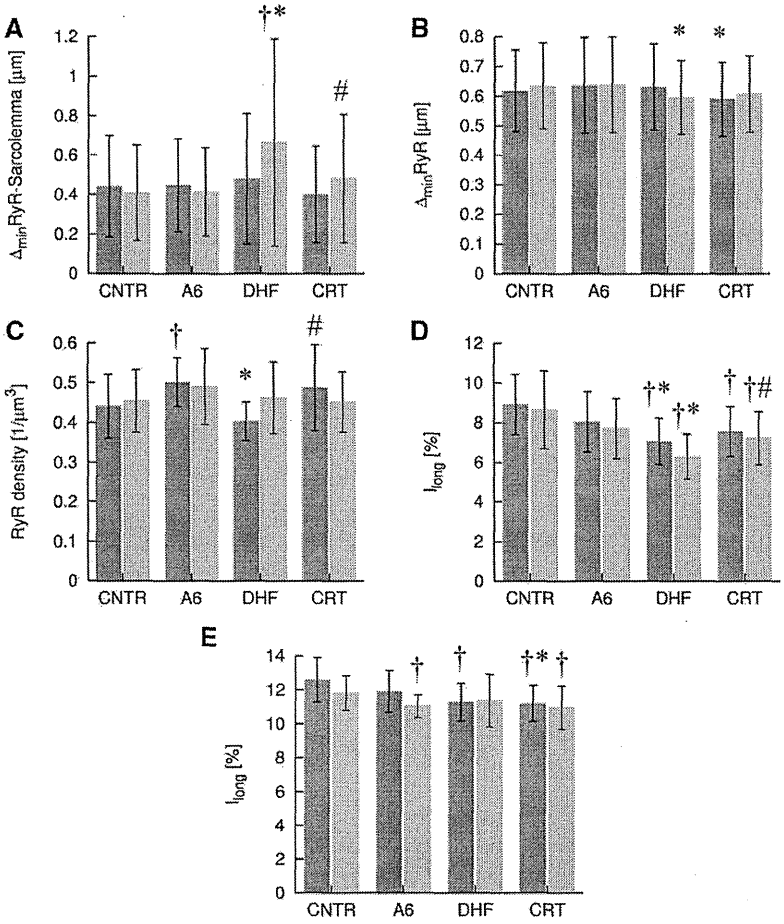

Figure 5. Structural characterization of control, DHF, and CRT cells. A, Distances of RyR clusters to closest sarcolemma. **B**, Nearest-neighbor distances of RyR cluster centers. **C**, Density of RyR clusters. The t-system and RyR arrangement were characterized in **D**, WGA, and **E**, RyR image stacks, respectively, by the normalized magnitudes of longitudinal frequency. †$P<0.05$ versus control, *$P<0.05$ versus A6, #$P<0.05$ versus DHF. Color coding as in Figure 4.

Maxima in the Fourier histogram from WGA images appear at similar sectors for images from CRT and DHF cells (Figure 4E). Also, the Fourier histograms from RyR images indicate that the arrangement of RyR clusters is similar in CRT and DHF cells of both types (Figure 4F versus Figure 3G).

Quantitative Analysis of the Effects of DHF and CRT on Subcellular Structure

A summary and statistical analysis of the results are presented in Figure 5. A striking marker of t-system remodeling is the RyR-sarcolemma distance (Figure 5A). In lateral myocytes, a significant increase is associated with DHF, which was substantially restored by CRT. Compared with control, neither DHF nor CRT caused alterations of the nearest-neighbor distance (Figure 5B). Differences of the density of RyR clusters were not significant for control versus DHF as well as A6 versus CRT (Figure 5C). The spatial arrangement of the t-system and RyR was characterized by the ratio of intensities associated with the longitudinal axis of cells to the overall intensities in the WGA and RyR image stacks, respectively. In comparison to control and A6, DHF was associated with a reduced longitudinal intensity ratio of WGA signals in both lateral and anterior cells (Figure 5D). This reduction indicates a less regular longitudinal spacing of the t-system in DHF. After CRT, the longitudinal intensity ratio was partially restored in lateral and anterior cells. However, in comparison to control, the longitudinal intensity ratio remained at reduced levels after CRT. DHF was associated with a slightly reduced longitudinal intensity ratio of RyR signals in anterior cells but not in lateral cells (Figure 5E). CRT cells exhibited a significant albeit small reduction of longitudinal intensity ratios of RyR signals in both cell types versus control. The differences between DHF and CRT cells were not significant, indicating that CRT was not able to restore the spatial arrangement of RyR clusters.

Analysis of Effects of DHF and CRT on Ca^{2+} Transients

Because we observed significant disorganization of structures associated with EC coupling in DHF, we expected reduced Ca^{2+} transients in the cardiomyocytes in which we found structural disorganization. We measured Ca^{2+} transients in the presence and absence of β-adrenergic stimulation with isoproterenol, which among other things increases the peak and time to peak of transients (Figure 6A). There was, as expected, a reduction of the Ca^{2+} transient peak (Figure 6B), increased time to peak (TTP) (Figure 6C), and slowed Ca^{2+} extrusion (Figure 6D and 6E) as a result of DHF regardless of whether or not cells were treated with isoproterenol. CRT

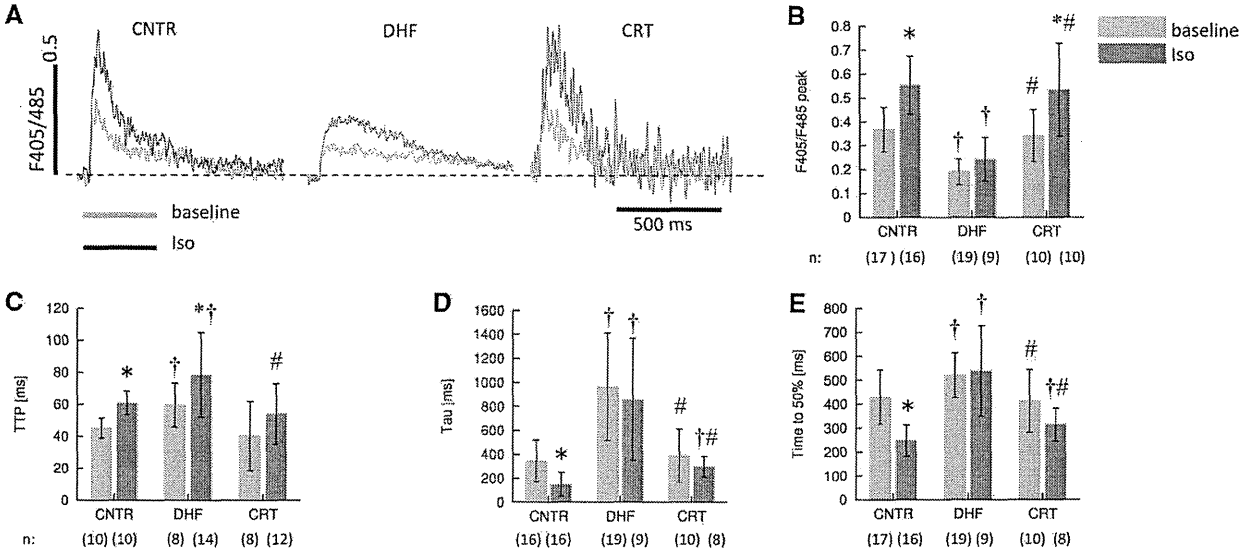

Figure 6. Characterization of Ca^{2+} transients in control, DHF, and CRT cells from lateral left ventricle. Ca^{2+} transients were evoked by field stimulation and measured by indo-1 fluorescence. **A**, Representative ratioed fluorescent signals at baseline and after application of isoproterenol. Analyses of these signals yielded **B**, peak amplitudes; **C**, time to peak (TTP); **D**, the time constant (tau) of the Ca^{2+} transient decay; and **E**, the time to 50% decay. DHF cells exhibit slowed and attenuated Ca^{2+} transients, which are normalized by CRT. †$P<0.05$ versus control, #$P<0.05$ versus DHF, *$P<0.05$ versus baseline. n, Number of cells.

restored the peak transient and TTP to values similar to those observed for control. Also, Ca^{2+} extrusion in CRT cells in the absence of β-adrenergic stimulation was accelerated versus DHF cells but not significantly different compared with control cells. This is consistent with the restoration of structure that we observed. Notably, our analysis revealed some differences between control and CRT cells in the presence of β-adrenergic stimulation. In the presence of isoproterenol, Ca^{2+} extrusion in CRT cells was slowed versus control. Also, CRT cells did not show a significant adrenergic response for the measures of Ca^{2+} extrusion.

Discussion

Despite the success of CRT in clinical treatment of patients with HF and cardiac dyssynchrony,[1,2] little is known about restoration of subcellular structures and functions related to EC coupling. Fluorescent labeling, 3D confocal microscopy, and image analysis provide a quantitative way of describing subcellular structures, their remodeling, and restoration. Using this approach, we demonstrated for the first time substantial remodeling of the t-system as a deleterious consequence of DHF and subsequent structural restoration of the t-system that result from CRT. In addition, we characterized the location of specific effects of DHF-associated structural remodeling of the t-system and its relationship to RyR clusters. Remodeling of t-tubules in DHF ranged from minor alterations in anterior left ventricular cells to nearly complete depletion in lateral cells. Our analyses did not reveal remodeling of the t-system by atrial tachypacing, indicating that remodeling in DHF is a consequence of cardiac dyssynchrony and its regional effects.

Ca^{2+} transients of cardiac myocytes are attenuated and Ca^{2+} extrusion is slowed in various models of HF, including our DHF model. We demonstrated previously that these alterations were particularly prominent in cells isolated from the lateral wall and that these features of Ca^{2+} transients were partially restored after CRT with more pronounced improvement in lateral cells.[11] We showed an increase of TTP for lateral DHF cells and restoration of TTP after CRT to control values. This restoration of Ca^{2+} transients is difficult to explain by changes of expression levels of proteins involved in Ca^{2+} signaling and their RNA messenger levels. $Ca_v1.2$ expression and messenger levels were not altered in DHF and after CRT.[11] RyR2 and SERCA2 levels declined in DHF and were not restored by CRT. A number of studies have demonstrated the depletion of the t-system in HF,[4–7] ischemia,[26] and cell culture.[27,28] Studies on cultured ovine myocytes demonstrated that as a result of t-tubular loss sparks are less synchronized.[28] This would significantly reduce the efficiency of EC coupling by among other things producing reduced and inhomogeneous Ca^{2+} transients. Because t-tubules and the associated RyR clusters are essential for normal EC coupling and Ca^{2+} transients are partially restored by CRT, we hypothesized that CRT would produce a restoration of the structure of the t-system and its relationship to RyRs. We suggest that the restoration revealed by our study can in part account for the restoration of Ca^{2+} transients that were observed as a result of CRT and are clearly essential for the restoration of function that is known to occur as a result of CRT.

In agreement with our results, several authors have demonstrated a loss or remodeling of t-tubules in HF. This is apparent in failing human heart[28,29] and has also been observed in other species, for example, in a murine model of myocardial infarction–induced congestive HF,[30] a rat model of aortic-banding–induced failure,[7] and a canine model based on tachypacing from an epicardial left ventricular site.[4,5] An exception appears in the results obtained by Ohler et al,[6] who did not observe statistically significant

loss of t-tubular surface area or volume in a study on a small number of failing human hearts with diverse conditions (2 hearts with dilated cardiomyopathy, 1 heart will familial cardiomyopathy, and 1 heart with ischemic cardiomyopathy). It is unclear what explains this exception or if the studied hearts exhibited electric or mechanical dyssynchrony. However, it is clear from a number of studies[28,30,31] that Ca^{2+} release appears to be delayed or asynchronous in cells from hearts progressing to or in failure. This is particularly apparent in the studies of Litwin et al[31] on myocytes from infarcted hearts. These authors observed highly asynchronous sparks and in the absence of structural studies this finding remains unexplained. In those cases in which asynchrony is associated with t-tubular loss, it probably is due to spatially inhomogeneous release of Ca^{2+}. Eventually, Ca^{2+} from couplons will spread to regions where release does not occur. This will amplify any asynchronous release of Ca^{2+} from couplons. Even if couplons are activated in a highly synchronous fashion, with missing release sites inhomogeneity of Ca^{2+} release from couplons will lead to the asynchronous appearance of Ca^{2+} in the cytosol. Inhomogeneous and/or asynchronous Ca^{2+} release in cells with reduced and/or disorganized t-tubules will reduce the cell's ability to shorten. In regions where sarcomeres are first exposed to Ca^{2+}, they will shorten. If they are in series with other sarcomeres that have not been exposed to Ca^{2+} because its appearance is delayed, the activated sarcomeres will shorten against the compliance of sarcomeres, which have not been activated. This will continue until either shortening of activated sarcomeres is complete or inactivated sarcomeres start to activate. This will have a tendency to reduce cellular shortening particularly if the effect is extensive. Gao et al[32] reported that cardiac force generation in intact ventricular tissue has an extremely steep dependence on Ca^{2+} with a Hill coefficient of 4.87. This steep relationship has been suggested to amplify effects of inhomogeneous Ca^{2+} delivery on cell shortening.[33] Indeed, Song et al[33] point out that at -30 mV, when local Ca^{2+} release events are asynchronous, cell shortening is barely detectable. This can explain the dramatic weakening of contraction that results from HF. Any mechanism that restores t-tubules will add homogeneity to cytosolic Ca^{2+} increases and has a disproportionately large effect on the restoration of shortening. Again, this is because the relationship between contractility and Ca^{2+} is steep. Thus a relatively modest restoration of t-tubules and release sites could have a pronounced effect on contractility. We assume that this is one reason for the efficacy of CRT.

Although we can clearly document depletion and disorganization of the t-system and, to a lesser extent, RyR clusters in DHF as well as their reorganization on CRT, the mechanisms underlying these alterations remain unclear. It is known that gene expression changes during HF,[34] and this change is to some extent restored during CRT.[15] Although the studies indicated that transcriptional alterations were particularly apparent in anterior cells, it is the late-activated lateral wall that undergoes the greatest stress in DHF and a major stress reduction during CRT via biventricular pacing. Changes in stress could in principle activate sarcolemmal stretch-activated ion channels and provide a signal, for example Ca^{2+}, that precipitates a cascade of events leading either to remodeling or restoration of the structures that we have studied. A similar effect could occur at the nuclear envelope, and it will be of interest to determine whether deformation of the nucleus by for example stretch precipitates ion fluxes (eg, Ca^{2+}) that could function as signals that ultimately lead to changes in genomic expression responsible for remodeling. An alternative possibility is that alterations in mechanical stress during DHF directly affect the structure of t-tubules and in turn directly influence the maintenance of t-system organization. This alternative is supported by studies demonstrating marked differences in strain profiles in DHF[11–13] and transmission of cellular strain to the t-system in ventricular myocytes.[35] Alterations of tissue strain (or stress) can be expected also in other models of HF, for instance, infarction and left ventricular tachypacing models, with demonstrated t-system remodeling.

We suggest that t-system restoration can serve as a complementary marker of CRT success. Assessment of CRT success will become even more important in the future as recommendations for CRT applications are extended for New York Heart Association classes I and II.[36] Because not all HF patients respond to CRT, an early marker of the benefit of CRT may inform decisions regarding continued pacing or alternative therapeutic strategies. By applying the labeling and imaging approaches that we described to cardiac biopsies, it should be possible to rapidly assess the efficacy of CRT.[21,37] Also, recently developed fiberoptic confocal microscopy in conjunction with established catheter technology may provide information on t-system organization of myocytes in situ.[38] However, limitations of this approach are associated with its invasiveness, and the effort needed, in particular, in comparison to established indices of resynchronization.

It should be recognized that in the model of CRT that we used mechanical synchrony is restored; however, tachycardia pacing is continued to maintain HF. Thus, in this study, t-system restoration does not coincide with the restoration of hemodynamic function during CRT (Online Table I). Hemodynamic function in CRT animals was in many aspects similar to animals undergoing 6 weeks of atrial tachypacing (A6). T-system restoration was apparent after 3 weeks in CRT. The restoration of the t-system architecture appears to be a marker of reduction in regional heterogeneity in loading and stress in the left ventricle rather than improvement in ventricular function per se. Our data suggest that the exaggerated differences in regional stresses have profound and direct effects on subcellular structure of myocytes. Moreover, these subcellular changes alter the spatial relationships of key components of Ca^{2+} signaling and are consistent with defects in Ca^{2+} transients observed in cells from DHF hearts. Remarkably, even in the context of ongoing HF, the subcellular changes in the high stress lateral wall of the left ventricle are reversible with restoration of electric and mechanical synchrony produced by CRT. The reversal of the subcellular structural

alterations not only contributes to improvement in Ca^{2+} homeostasis but might also arrest the progression in the HF phenotype in patients that respond to CRT.

Acknowledgments

We thank Deborah DiSilvestre and Dr Philip R. Ershler for expert technical assistance. We thank Dr Kenneth Spitzer for useful discussions.

Sources of Funding

The study was supported by NIH grants R01 HL094464 (F.B.S.) and PO1 HL077180 (D.A.K., G.F.T., T.A) and the Richard A. and Nora Eccles Fund for Cardiovascular Research and awards from the Nora Eccles Treadwell Foundation (J.H.B., F.B.S.).

Disclosures

Dr Kass has served as a consultant to or on the advisory board of Boston Scientific Consulting.

References

1. Cleland JG, Daubert JC, Erdmann E, Freemantle N, Gras D, Kappenberger L, Tavazzi L. The effect of cardiac resynchronization on morbidity and mortality in heart failure. *N Engl J Med.* 2005;352:1539–1549.
2. Bristow MR, Saxon LA, Boehmer J, Krueger S, Kass DA, De Marco T, Carson P, DiCarlo L, DeMets D, White BG, DeVries DW, Feldman AM. Cardiac-resynchronization therapy with or without an implantable defibrillator in advanced chronic heart failure. *N Engl J Med.* 2004;350: 2140–2150.
3. Iuliano S, Fisher SG, Karasik PE, Fletcher RD, Singh SN. QRS duration and mortality in patients with congestive heart failure. *Am Heart J.* 2002;143:1085–1091.
4. He JQ, Conklin MW, Foell JD, Wolff MR, Haworth RA, Coronado R, Kamp TJ. Reduction in density of transverse tubules and l-type Ca2+ channels in canine tachycardia-induced heart failure. *Cardiovasc Res.* 2001;49:298–307.
5. Balijepalli RC, Lokuta AJ, Maertz NA, Buck JM, Haworth RA, Valdivia HH, Kamp TJ. Depletion of t-tubules and specific subcellular changes in sarcolemmal proteins in tachycardia-induced heart failure. *Cardiovasc Res.* 2003;59:67–77.
6. Ohler A, Weisser-Thomas J, Piacentino V, Houser SR, Tomaselli GF, O'Rourke B. Two-photon laser scanning microscopy of the transverse-axial tubule system in ventricular cardiomyocytes from failing and non-failing human hearts. *Cardiol Res Pract.* 2009:802373, 2009.
7. Wei S, Guo A, Chen B, Kutschke W, Xie YP, Zimmerman K, Weiss RM, Anderson ME, Cheng H, Song LS. T-tubule remodeling during transition from hypertrophy to heart failure. *Circ Res.* 2010;107:520–531.
8. Louch WE, Sejersted OM, Swift F. There goes the neighborhood: pathological alterations in t-tubule morphology and consequences for cardiomyocyte Ca2+ handling. *J Biomed Biotechnol.* 2010;2010: 503906.
9. Brillantes A-M, Allen P, Takahashi T, Izumo S, Marks AR. Differences in cardiac calcium release channel (ryanodine receptor) expression in myocardium from patients with end- stage heart failure caused by ischemic versus dilated cardiomyopathy. *Circ Res.* 1992;71:18–26.
10. Reinecke H, Studer R, Better R, Just H, Holtz J, Drexler H. Enhanced expression and function of the cardiac sodium-calcium exchanger in end-stage human heart failure. *Circulation.* 1993;88:I-408.
11. Aiba T, Hesketh GG, Barth AS, Liu T, Daya S, Chakir K, Dimaano VL, Abraham TP, O'Rourke B, Akar FG, Kass DA, Tomaselli GF. Electrophysiological consequences of dyssynchronous heart failure and its restoration by resynchronization therapy. *Circulation.* 2009; 119:1220–1230.
12. Chakir K, Daya SK, Aiba T, Tunin RS, Dimaano VL, Abraham TP, Jaques-Robinson KM, Lai EW, Pacak K, Zhu WZ, Xiao RP, Tomaselli GF, Kass DA. Mechanisms of enhanced beta-adrenergic reserve from cardiac resynchronization therapy. *Circulation.* 2009;119:1231–1240.
13. Chakir K, Daya SK, Tunin RS, Helm RH, Byrne MJ, Dimaano VL, Lardo AC, Abraham TP, Tomaselli GF, Kass DA. Reversal of global apoptosis and regional stress kinase activation by cardiac resynchronization. *Circulation.* 2008;117:1369–1377.
14. Chakir K, Depry C, Dimaano VL, Zhu WZ, Vanderheyden M, Bartunek J, Abraham TP, Tomaselli GF, Liu SB, Xiang YK, Zhang M, Takimoto E, Dulin N, Xiao RP, Zhang J, Kass DA. Galphas-biased beta2-adrenergic receptor signaling from restoring synchronous contraction in the failing heart. *Sci Transl Med.* 2011;3:100–188.
15. Barth AS, Aiba T, Halperin V, DiSilvestre D, Chakir K, Colantuoni C, Tunin RS, Dimaano VL, Yu W, Abraham TP, Kass DA, Tomaselli GF. Cardiac resynchronization therapy corrects dyssynchrony-induced regional gene expression changes on a genomic level. *Circ Cardiovasc Genet.* 2009;2:371–378.
16. Nelson DA, Benson ES. On the structural continuities of the transverse tubular system of rabbit and human myocardial cells. *J Cell Biol.* 1963; 16:297–313.
17. Fawcett DW, McNutt NS. The ultrastructure of the cat myocardium, I: ventricular papillary muscle. *J Cell Biol.* 1969;42:1–45.
18. Brette F, Orchard C. T-tubule function in mammalian cardiac myocytes. *Circ Res.* 2003;92:1182–1192.
19. Franzini-Armstrong C, Protasi F, Ramesh V. Shape, size, and distribution of Ca(2+) release units and couplons in skeletal and cardiac muscles. *Biophys J.* 1999;77:1528–1539.
20. Stern MD, Lakatta EG. Excitation-contraction coupling in the heart: the state of the question. *FASEB J.* 1992;6:3092–3100.
21. Savio-Galimberti E, Frank J, Inoue M, Goldhaber JI, Cannell MB, Bridge JH, Sachse FB. Novel features of the rabbit transverse tubular system revealed by quantitative analysis of three-dimensional reconstructions from confocal images. *Biophys J.* 2008;95:2053–2062.
22. Spragg DD, Akar FG, Helm RH, Tunin RS, Tomaselli GF, Kass DA. Abnormal conduction and repolarization in late-activated myocardium of dyssynchronously contracting hearts. *Cardiovasc Res.* 2005;67:77–86.
23. Leclercq C, Faris O, Tunin R, Johnson J, Kato R, Evans F, Spinelli J, Halperin H, McVeigh E, Kass DA. Systolic improvement and mechanical resynchronization does not require electrical synchrony in the dilated failing heart with left bundle-branch block. *Circulation.* 2002;106: 1760–1763.
24. Sachse FB, Savio-Galimberti E, Goldhaber JI, Bridge JH. Towards computational modeling of excitation-contraction coupling in cardiac myocytes: reconstruction of structures and proteins from confocal imaging. *Pac Symp Biocomput.* 2009:328–339.
25. O'Rourke B, Kass DA, Tomaselli GF, Kaab S, Tunin R, Marban E. Mechanisms of altered excitation-contraction coupling in canine tachycardia-induced heart failure, I: experimental studies. *Circ Res.* 1999; 84:562–570.
26. Heinzel FR, Bito V, Biesmans L, Wu M, Detre E, von Wegner F, Claus P, Dymarkowski S, Maes F, Bogaert J, Rademakers F, D'Hooge J, Sipido K. Remodeling of t-tubules and reduced synchrony of Ca2+ release in myocytes from chronically ischemic myocardium. *Circ Res.* 2008;102: 338–346.
27. Mitcheson JS, Hancox JC, Levi AJ. Action potentials, ion channel currents and transverse tubule density in adult rabbit ventricular myocytes maintained for 6 days in cell culture. *Pflugers Arch.* 1996; 431:814–827.
28. Louch WE, Bito V, Heinzel FR, Macianskiene R, Vanhaecke J, Flameng W, Mubagwa K, Sipido KR. Reduced synchrony of Ca2+ release with loss of t-tubules: a comparison to Ca2+ release in human failing cardiomyocytes. *Cardiovasc Res.* 2004;62:63–73.
29. Crossman DJ, Ruygrok PR, Soeller C, Cannell MB. Changes in the organization of excitation-contraction coupling structures in failing human heart. *PLoS One.* 2011;6:e17901.
30. Louch WE, Mork HK, Sexton J, Stromme TA, Laake P, Sjaastad I, Sejersted OM. T-tubule disorganization and reduced synchrony of Ca2+ release in murine cardiomyocytes following myocardial infarction. *J Physiol.* 2006;574:519–533.
31. Litwin SE, Zhang D, Bridge JH. Dyssynchronous Ca(2+) sparks in myocytes from infarcted hearts. *Circ Res.* 2000;87:1040–1047.
32. Gao WD, Backx PH, Azan-Backx M, Marban E. Myofilament Ca^{2+} sensitivity in intact versus skinned rat ventricular muscle. *Circ Res.* 1994;74:408–415.
33. Song LS, Wang SQ, Xiao RP, Spurgeon H, Lakatta EG, Cheng H. Beta-adrenergic stimulation synchronizes intracellular Ca(2+) release

during excitation-contraction coupling in cardiac myocytes. *Circ Res.* 2001;88:794–801.
34. Kittleson MM, Minhas KM, Irizarry RA, Ye SQ, Edness G, Breton E, Conte JV, Tomaselli G, Garcia JG, Hare JM. Gene expression analysis of ischemic and nonischemic cardiomyopathy: shared and distinct genes in the development of heart failure. *Physiol Genom.* 2005;21: 299–307.
35. McNary TG, Bridge JH, Sachse FB. Strain transfer in ventricular cardiomyocytes to their transverse tubular system revealed by scanning confocal microscopy. *Biophys J.* 2011;100:L53–L55.
36. Linde C, Daubert C. Cardiac resynchronization therapy in patients with New York Heart Association class I and II heart failure: an approach to 2010. *Circulation.* 2010;122:1037–1043.
37. Soeller C, Cannell MB. Examination of the transverse tubular system in living cardiac rat myocytes by 2-photon microscopy and digital image-processing techniques. *Circ Res.* 1999;84:266–275.
38. Lasher RA, Hitchcock RW, Sachse FB. Towards modeling of cardiac micro-structure with catheter-based confocal microscopy: a novel approach for dye delivery and tissue characterization. *IEEE Trans Med Imaging.* 2009;28:1156–1164.

Novelty and Significance

What Is Known?

- Cardiac resynchronization therapy (CRT) reduces symptoms and mortality in patients affected by dyssynchronous heart failure (DHF).
- DHF is caused by dyssynchronous electric and mechanical activation of the left and right ventricle.
- Remodeling of electrophysiological properties, hemodynamics, and protein expression due to DHF is partially restored by CRT.

What New Information Does This Article Contribute?

- DHF is associated with structural remodeling of the transverse tubular system (t-system) and its spatial relationship to ryanodine receptor clusters in lateral left ventricular myocytes, which also exhibited reduced and slowed calcium transients.
- After CRT, we found restoration of the t-system, its spatial relationship to ryanodine receptor clusters, and the calcium transient.
- A heart failure model based on tachypacing did not exhibit significant depletion and disorganization of the t-system, suggesting that dyssynchrony underlies changes that we found in DHF.

This study was designed to investigate subcellular remodeling underlying DHF and CRT in a large-animal model. We applied scanning confocal microscopy to generate 3D reconstructions of the t-system and ryanodine receptor clusters in segments of isolated cells. Analyses of reconstructions of DHF cells revealed regional depletion and disorganization of the t-system and alterations of its spatial relationship to ryanodine receptor clusters. These structures were restored by CRT. Structural remodeling and restoration were accompanied with remodeling and restoration of calcium transients. Our approach opens the possibility of investigating the causes of remodeling of subcellular structure after DHF and CRT, including changes in genome expression and protein distributions as well as alterations in mechanical stress. Our findings suggest that the organization of t-system can provide an early marker for the success of CRT.

Current Topics

Stem Cell Research for Regenerative Medicine/Personalized Medicine

Novel Insights into Disease Modeling Using Induced Pluripotent Stem Cells

Toru Egashira, Shinsuke Yuasa, and Keiichi Fukuda*

Department of Cardiology, Keio University School of Medicine; 35 Shinanomachi, Shinjuku-ku, Tokyo 160–8582, Japan.

Received October 31, 2012

Induced pluripotent stem cell (iPSC) technology has great potential to establish novel therapeutic approaches in regenerative medicine and disease analysis. Although cell therapy using iPSC-derived cells still has many hurdles to overcome before clinical applications, disease analysis using patient-specific iPSCs may be of practical use in the near future. There are several reports that patient-specific iPSC-derived cells have recapitulated the apparent cellular phenotypes of a wide variety of diseases. Moreover, some studies revealed that it could be possible to discover effective new drugs and to clarify disease pathogenesis by examination of patient-specific iPSC-derived cells *in vitro*. We have recently reported that iPSCs can be a diagnostic tool in a patient with a novel mutation. For definitive diagnosis in a patient with long QT syndrome who had an uncharacterized genetic mutation, we succeeded in clarifying the patient's cellular electrophysiologic characteristics and the molecular mechanism underlying the disease phenotype through the multifaceted analyses of patient-specific iPSC-derived cardiomyocytes. In this review, we focus on the conceptual and practical issues in disease modeling using patient-specific iPSCs and discuss future directions in this research field.

Key words induced pluripotent stem cell; disease modeling; cardiovascular disease; long QT syndrome

1. INTRODUCTION

Induced pluripotent stem cells (iPSCs) are defined as artificial pluripotent stem cells that can be generated from somatic cells by introducing reprogramming factors (*e.g.*, *OCT3/4*, *SOX2*, *KLF4*, *c-MYC*, *NANOG*, and *LIN28*).[1,2] The methodology for generating iPSCs has markedly improved and now integration-free iPSCs, without transgene insertion in the host genome, can be obtained using several procedures.[3–7] iPSCs maintain the two essential stem cell characteristics of infinite self-renewal capability and pluripotency, meaning that they can give rise to all cell types of the three germ layers and differentiate in a fashion similar to normal embryogenesis.[8,9]

One of the expectations of iPSCs is the generation of human disease-specific pluripotent stem cells from patients. Such iPSCs, refered to as patient-specific iPSCs, can differentiate into any type of cell including a patient's diseased organ tissue, and the genetic information of patient-specific iPSCs is identical to that of the patient.[10] Therefore we can directly and repetitively analyze diseased cells using patient-specific iPSC-derived cells. Figure 1 shows the conceptual scheme for the utilization of patient-specific iPSCs in clinical practice. To date, many groups have reported that the apparent cellular phenotypes of genetic disorders can be recapitulated in patient-specific iPSC-derived cells *in vitro* (Table 1). Some reports also involved drug screening using iPSCs, resulting in the proposal of novel drug candidates.[11,12] We have recently reported that functional analyses of patient-specific iPSC-derived cardiomyocytes elucidated the molecular mechanism of the disease phenotype in a patient with undiagnosed sporadic long QT syndrome (LQTS).[13] This paper reviews current topics in disease modeling using patient-specific iPSCs and introduces our study as an actual example in this research field.

2. GENERATION OF PATIENT-SPECIFIC iPSCs

Disease Selection Although any type of disease can theoretically be reproduced by patient-specific iPSC-derived cells, in many diseases it appears difficult to recapitulate the phenotype using this technique because of problems related to both the properties of iPSCs and the disease causality. First, the differentiation efficiency of iPSCs into specific cells restricts the category of disease.[14] In terms of the maturity of iPSC-derived cells, it may be easier to to reproduce the phenotype of disease occurring in younger individuals because of the immaturity of iPSC-derived cells.[15] Disease mainly caused by the alteration of epigenetic status due to environmental parameters is not suitable for modeling using iPSCs because the cellular epigenetic information can be partly renewed during the process of reprogramming.[16,17] On the other hand, in disease directly caused by a genetic aberration that is clearly preserved in iPSCs, it is feasible to confirm whether patient-specific iPSC-derived cells can reproduce diseased cellular kinetics. In addition, apparent phenotypes can be determined even at the single-cell level because of the difficulty in organ formation from iPSCs.[18]

Considering those issues comprehensively, the first disease to be analyzed using patient-specific iPSCs should be a monogenetic disorder with severe phenotypes diagnosed in infancy and easily examined with simple methods at the single-cell level. Most studies using patient-specific iPSCs focus on diseases that satisfy such requirements. LQTS was selected by

The authors declare no conflict of interest.

* To whom correspondence should be addressed. e-mail: kfukuda@a2.keio.jp

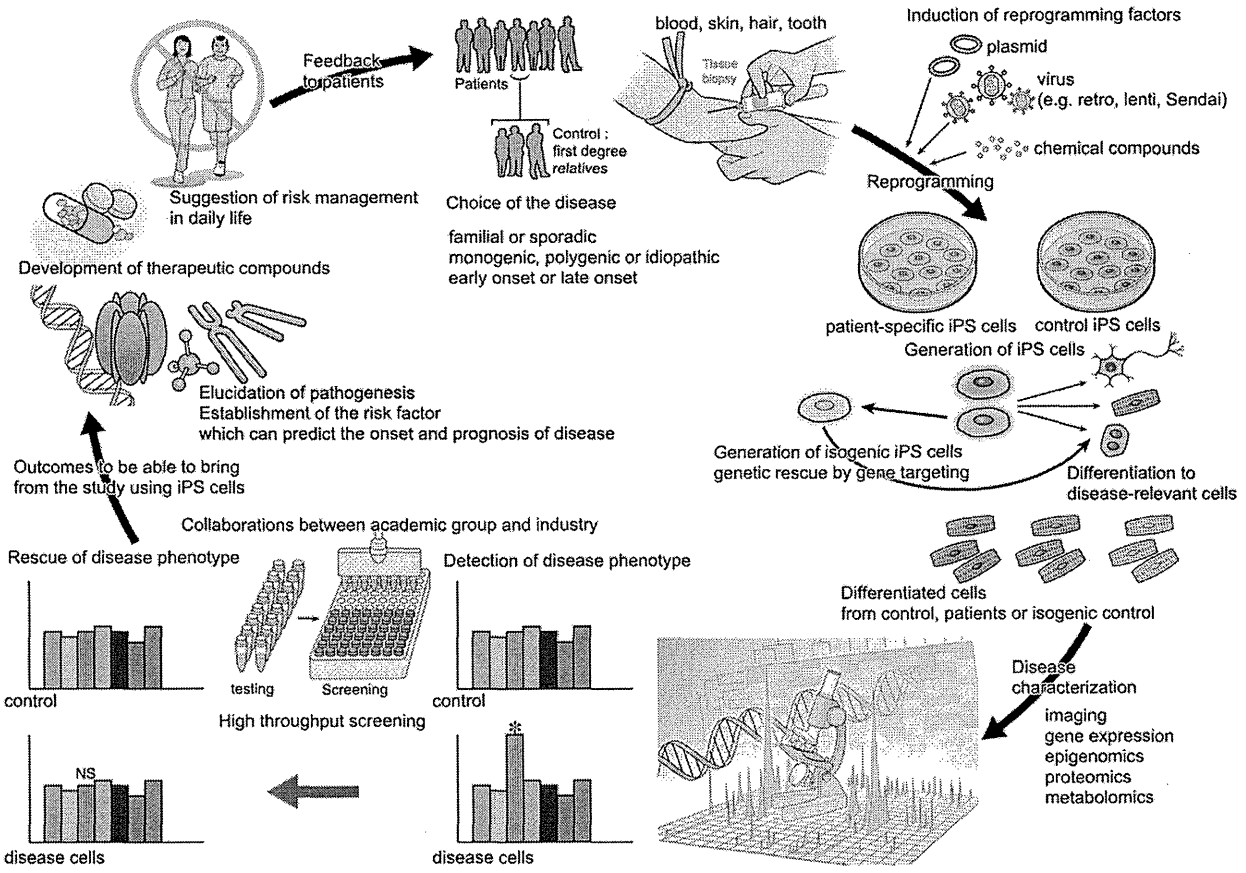

Fig. 1. Overview of Issues in Clinical Applications Using Patient-Specific iPSC Technology

This scheme shows the circle that is one model of patient-specific iPSC technology. The disease type was selected from among many conditions. Controls are often first-degree relatives of patients. Somatic cells are obtained from the blood, skin, hair, or teeth and then reprogramming factors are introduced using various methods (*e.g.*, plasmid, virus, or chemical compounds) and both patient-specific and control iPSCs are generated. If possible, isogenic control iPSCs could be generated through genetic rescue by gene targeting. After evaluating the quality of iPSCs generated, they are differentiated into disease-relevant cells. Then both types of iPSC-derived cell are characterized using various techniques (imaging, genomics, epigenomics, proteomics, metabolomics, *etc.*). Based on the results of pioneering studies, further examinations such as high-throughput screening using large chemical libraries are planned through collaborations between academic research groups and pharmaceutical companies. Expected results of studies on iPSCs are the development of novel therapeutic compounds, establishment of novel risk factors predicting the onset of disease and prognosis, and suggestions on appropriate lifestyles which can serve as feedback to patients.

our and other groups as a disease model using patient-specific iPSCs. LQTS is an inherited life-threatening disease caused by functional impairment of the cardiac ion channel with a monogenetic aberration and often causes sudden cardiac death due to ventricular tachyarrhythmia even in infancy.[19,20]

Derivation and Characterization of Patient-Specific iPSCs Originally, iPSCs were generated from dermal fibroblasts in a retroviral transduction system.[1,21] Subsequently, the methodology for generating iPSCs rapidly improved and became simpler and more efficient, enabling the generation of iPSCs using less patient-invasive methods. Moreover, using plasmid vectors, RNA viruses, and other methods, good-quality iPSCs can be obtained without the need for integrating reprogramming factors.[3–7] Integration-free iPSCs appear ideal because exogenous genes integrated in the host genome may affect the genetic properties of the iPSCs generated and modify the cellular phenotypes of patient-specific iPSC-derived cells.[22]

We previously reported that integration-free iPSCs can be efficiently, easily, and rapidly generated from terminally differentiated circulating T lymphocytes in peripheral blood using Sendai virus (RNA virus).[23] Our method makes it possible to generate iPSCs from any patient including infants, girls, and the very elderly *via* simple blood sampling, which is one of the least-invasive common clinical procedures. Such cumulative progress in generating iPSCs can accelerate the widespread application of patient-specific iPSC technology.

Before the utilization of generated iPSCs in disease modeling, their characteristics must be evaluated.[24] It should be determined whether problems occurred during iPSC reprogramming and maintenance, such as the occurrence of somatic coding mutations,[25] dynamic changes in the allelic copy number variation,[26] abnormality of X chromosome inactivation,[27] incomplete demethylation,[28] *etc.* These elements may affect the phenotype of iPSC-derived cells and skew the interpretation of the results of their assay. In addition, the most appropriate control group remains controversial. In most previous studies, the control groups comprised healthy volunteers without genetic mutations who were unrelated to or relatives of the patients involved. It remains unclear which controls are optimal in disease modeling using patient-specific iPSCs. To examine the unadulterated functions of mutated genes, it appears preferable to compare patients with family members who do not carry the mutation, although related

Table 1. Summary of the Literature on Disease Modeling Using Patient-Specific iPSCs

Disease	Gene mutation	Cell type	Cellular phenotype	Refs.
AD	PS1 mutations	Neurons	Increase in Aβ secretion and rescued by γ-secretase inhibitors	44)
PD	LRRK2 mutations	Neurons-dopaminergic	Degeneration due to increased oxidative-stress	45)
CPVT	RYR2 mutations	Cardiomyocytes	Abnormal dynamism in Ca handling and treatment with several drugs rescues the phenotype	46)
DCM	TNNT2 mutations	Cardiomyocytes	Altered regulation of Ca emphasized by β adrenergic agonist and rescued by β blocker	47)
FH	LDL receptor mutations	Hepatocytes	Impaired ability to incorporate LDL	48)
CML	BCR-ABL	iPSCs, Hematopoietic cells	Imatinib resistant in iPSCs and immature Hematopoietic cells	49)
MD (+DM)	mtDNA A3243G mutation	iPSCs, EBs	Variety of degree of mutation heteroplasmy in each iPSC clones	50)
DS (+AD)	Trisomy 21	Neurons-cortical	Secretion of the pathogenic peptide fragment amyloid-β42	51)
DKC	DKC1, TERT, TCAB1 mutation	iPSCs	Progressive telomere shortening and loss of self-renewal of iPSCs	52), 53)
RP	RP1, RP9, PRPH2, RHO mutations	Rod photoreceptor cells	Decreased numbers of differentiated rod cells and expression of cellular stress markers	54)
GD	GCase mutations	Neurons-dopaminergic	Lysosomal protein degradation, causes accumulation of α-synuclein	55)

AD: Alzheimer's Disease, PD: Parkinson's Disease, CPVT: Catecholaminergic Polymorphic Ventricular Tachycardia, DCM: Dilated Cardiomyopathy, FH: Familial Hypercholesterolemia, CML: Clonic Myeloid Leukemia, MD: Mitochondrial Disease, DM: Diabetes Mellitus, DS: Down Syndrome, DKC: Dyskeratosis Congenita, RP: Retinitis Pigmentosa, GD Gaucher Disease.

family members partly share genetic information including single-nucleotide polymorphisms, and this could affect disease phenotype. A recent study has demonstrated that ideal control iPSCs can be obtained by mutated gene correction using a targeting strategy.[29,30] Even though it cannot be applied in every disease model, further analysis using isogenic-control iPSCs may be the answer to this problem.

Differentiation into Disease Relevant-Cells iPSCs can give rise to a wide variety of cell types present in the three germ layers. In most cases, differentiation methods for iPSCs are applied with some modification from the methods established in embryonic stem cells, which are similar to the regulatory mechanisms of normal early development.[8,9] To establish methods for *in vitro* differentiation from pluripotent stem cells, various screening methods for essential signaling molecules in normal development have been performed.[31]

Among several iPSC lines, the variation in differentiation propensity into specific cell types is well known.[32,33] Therefore the cell type of each iPSC generated should be confirmed before selecting the optimal cell line that can most efficiently differentiate into the cells of interest. A recent study has shown that iPSCs maintain epigenetic memories originally belonging to somatic cells, and this epigenetic status can regulate the characteristics of iPSCs, especially their differentiation propensity.[34–36] Therefore it is important to confirm which cells are the best source for iPSCs to obtain stable, disease-relevant cells.

To investigate more sophisticated experimental conditions similar to the physiologic environment, further improvements are required. First, it is necessary to establish a procedure to purify the cells from aggregations of iPSC-derived miscellaneous cells.[37,38] In addition, it would be ideal to be able to differentiate iPSCs into all constitutive cell types of an organ. In other words, to create organs *in vitro*, not only a single specific cell type but also other cell types such as endothelial cells, fibroblasts, and peripheral neural cells are needed. Furthermore, there are various subpopulations among cardiomyocytes such as atrial-, nodal- and ventricular-type cardiomyocytes, although at present there is no method to obtain each specific cell type.[39] These are crucial limitations on the reliability of results of the novel iPSC assay. In addition, iPSC-derived cells retain the original fetal-like characteristics, and it remains unclear how these cells can be appropriately matured.[40] Still another unresolved issue is the best time in the developmental stage of patient-specific iPSC-derived cells to analyze cellular function in terms of disease properties.

A recent advance in reprogramming to change the cellular fate is direct conversion, which allows terminally differentiated cells to be transformed into other functional cells of different lineages without passing through the pluripotent state.[41,42] In this method, mature target cells can be obtained within a shorter period, and disease modeling using this direct conversion technique has also been reported.[43] However, in spite of lower induction efficiency and the lack of a method established for all cell lineages, iPSCs seem to be a suitable cell source for disease modeling. The infinite self-renewability of iPSCs allows repetitive, reproducible analysis of the disease cells of interest.

Disease Modeling Using Patient-Specific iPSCs To date, several patient-specific iPSC lines have been generated from patients with a wide variety of mainly monogenetic, early-onset diseases such as neurologic disorders,[44,45] heart disease,[46,47] metabolic disease,[48] hematologic disorders,[49] mitochondrial disease,[50] chromosomal abnormalities,[51] telomere disease,[52,53] sensory organ disorder,[54] and storage disease.[55] The current list of studies of disease modeling using patient-specific iPSCs is shown in Table 1. While findings on patient-specific iPSCs have accumulated, analysis becomes more complicated in polygenic, sporadic, late-onset disease.[12,56,57] The next steps that will deliver useful clinical information resulting from patient-specific iPSC technology will result from collaborations between academic research groups and

pharmaceutical companies, which are expected develop novel therapeutic compounds and clarify possible sife effects through advanced high-throughput screening systems using patient-specific iPSC-derived cells.

3. CARDIOVASCULAR DISEASE MODELING USING iPSCs

Functional Characteristics of iPSC-Derived Cardiomyocytes On the premise that the study of human cardiovascular disease modeling will be initiated using patient-specific iPSCs, it is necessary to confirm that the characteristics of human iPSC-derived cardiomyocytes are physiologically analogous to human cardiomyocytes *in vivo*. Previous molecular biological and physiologic studies revealed that iPSC-derived cardiomyocytes have normal cardiomyocyte functional properties.[58,59] iPSC-derived cardiomyocytes have a striated muscle structure identical to that of normal functional cardiomyocytes and express cardiac-specific proteins, as confirmed in molecular biological assays such as immunocytochemistry and reverse-transcriptase polymerase chain reaction (PCR). Based on the waveform of the action potential, iPSC-derived cardiomyocytes can be divided into three subpopulations: atrial, nodal, and ventricular cells. Moreover, the contraction of iPSC-derived cardiomyocytes is regulated by physiologic intracellular signaling including excitation-contraction coupling,[60] and those cardiomyocytes express typical ion channels with the expected functional responses to several ion channel blockers.[61] All these findings indicate the validity of studies that will lead to the analysis of cardiovascular disease using patient-specific iPSC-derived cardiomyocytes.

Modeling LQTS Type 1 Some groups thought that LQTS would be a suitable disease for modeling using iPSCs because of the promising reproducibility of disease phenotypes in iPSC-derived cardiomyocytes.[13,62–67] Moretti *et al.* first showed that patient-specific iPSC-derived cardiomyocytes could recapitulate the disease phenotype in congenital LQTS.[62] They generated iPSCs from two patients with LQTS type 1, who had autosomal-dominant inheritance of a G569A missense mutation in the *KCNQ1* gene encoding the IKs current which was previously shown to be relevant to LQTS onset by functional analysis of the mutated gene.[68]

Individual cardiomyocytes derived from LQTS type 1 patient-specific iPSCs (LQTS1-iPSC-CMs) showed prolonged action potentials using whole-cell patch clamping compared with cardiomyocytes from healthy control donors who were unrelated to the patients. Moreover, LQTS1-iPSC-CMs exhibited increased susceptibility to catecholamine-induced tachyarrhythmia, which is one of the most important clinical features of the syndrome.[69] Even though that study was recognized as an important work first confirming the great potential of patient-specific iPSCs, we thought that there was room for expansion of the scope. In not only that study but also in other reports of LQTS disease modeling using iPSCs, patients who had mutated channel profiles characterized by conventional experimental methods were selected. In reality, many patients have unknown mutations that give no specific information on their disease phenotype. To address whether iPSC technology could be used to characterize the disease phenotype with a novel mutated gene, we selected LQTS patients with no family history or previous disease characterization.[13]

We generated iPSCs from a 13-year-old boy who was a sporadic LQTS patient. He had survived cardiopulmonary arrest due to ventricular fibrillation, and his subtype of LQTS could not be diagnosed using standard clinical tests.[70,71] Two healthy volunteers served as controls who donated iPSCs that had differentiated into cardiomyocytes. Our patient had a novel heterozygous mutation located in the *KCNQ1* gene, 1893delC, identified by genotyping of his blood sample.[72] Electrophysiologic function was measured using a multielectrode array system,[73] which showed that the duration of the field potential was markedly prolonged in LQTS-iPSCs-CMs as compared with cardiomyocytes derived from controls, which suggested that LQTS-iPSC-CMs maintained the patient's characteristics and could be successfully reproduced in this assay system.

Next we tried to confirm the responsible channel for the disease phenotype by precise evaluation of several drug responses. We clarified that the IKs channel was functionally impaired and that the IKr channel could compensate for this effect in LQTS-iPSC-CMs with the administration of several potassium current blockers. In general, the IKr and IKs channels work in a complementary fashion in the repolarization of cardiomyocytes, which is known as the repolarization reserve,[74] and we confirmed that this mechanism regulated the balance of the potassium current in LQTS-iPSC-CMs. Arrhythmogenic events in LQTS-iPSC-CMs caused by adrenergic stimulation also suggested that the patient's IK channel was significantly attenuated.[70,71] These findings strongly suggested that cardiomyocytes in the patient's IKs channel were functionally impaired and that the precise diagnosis was LQTS type 1.[75] To confirm the dominant-negative role of the *KCNQ1* 1893delC mutation in IKs channel function, we performed electrophysiologic and histochemical analyses in iPSC-derived cardiomyocytes and found that *KCNQ1* 1893delC has a dominant-negative effect *via* a trafficking deficiency.

Importantly, our study demonstrated that iPSCs could be useful to characterize the electrophysiologic cellular phenotype of a patient with a novel mutation. We performed functional analysis of the novel mutation using patient-specific iPSCs, which may support the diagnosis of LQTS type 1. Moreover, this system allowed us to perform several drug administration tests on LQTS-iPSC-CMs, which would be extremely risky to such a patient in clinical practice.[76] Therefore patient-specific iPSC technology can be used for drug evaluation and monitoring. At the same time, we were able to clarify the underlying molecular mechanism of the disease phenotype using this assay system.

4. CONCLUSION

Although iPSC technology is an attractive tool for analyzing human genetic diseases, it is clear that technological innovation remains necessary for the utilization of iPSCs in routine medical practice. Disease modeling using patient-specific iPSCs is a novel procedure for analyzing disease. It enables a direct, repetitive approach to diseased cells and has great potential to elucidate novel disease pathogenesis and develop new therapeutic compounds. However, in terms of the effort, cost, and time required in current studies using iPSCs, routine clinical usage is not yet feasible.[77] In addition, improvement of the quality of iPSCs and iPSC-derived cells is required

to make disease models using iPSCs more faithful. Some problems such as genetic mutations during reprogramming, incomplete epigenetic reprogramming, and undesired gene expression should also be controlled and standardized. More sophisticated differentiation, maturation, and purification protocols will be indispensable to create physiologic cellular conditions that reflect the actual disease phenotype.

In conclusion, steady progress is being made in iPSC technology to overcome the hurdles, and disease modeling using iPSCs appears a likely technique for the future. Recent and future innovations in the technique hold out the promise of patient-derived iPSC technology to achieve personalized medicine in the clinical setting.

REFERENCES

1) Takahashi K, Tanabe K, Ohnuki M, Narita M, Ichisaka T, Tomoda K, Yamanaka S. Induction of pluripotent stem cells from adult human fibroblasts by defined factors. *Cell*, **131**, 861–872 (2007).
2) Yu J, Vodyanik MA, Smuga-Otto K, Antosiewicz-Bourget J, Frane JL, Tian S, Nie J, Jonsdottir GA, Ruotti V, Stewart R, Slukvin II, Thomson JA. Induced pluripotent stem cell lines derived from human somatic cells. *Science*, **318**, 1917–1920 (2007).
3) Yu J, Hu K, Smuga-Otto K, Tian S, Stewart R, Slukvin II, Thomson JA. Human induced pluripotent stem cells free of vector and transgene sequences. *Science*, **324**, 797–801 (2009).
4) Kim D, Kim C-H, Moon J-I, Chung YG, Chang MY, Han BS, Ko S, Yang E, Cha KY, Lanza R, Kim KS. Generation of human induced pluripotent stem cells by direct delivery of reprogramming proteins. *Cell Stem Cell*, **4**, 472–476 (2009).
5) Ban H, Nishishita N, Fusaki N, Tabata T, Saeki K, Shikamura M, Takada N, Inoue M, Hasegawa M, Kawamata S, Nishikawa S. Efficient generation of transgene-free human induced pluripotent stem cells (iPSCs) by temperature-sensitive Sendai virus vectors. *Proc. Natl. Acad. Sci. U.S.A.*, **108**, 14234–14239 (2011).
6) Warren L, Manos PD, Ahfeldt T, Loh YH, Li H, Lau F, Ebina W, Mandal PK, Smith ZD, Meissner A, Daley GQ, Brack AS, Collins JJ, Cowan C, Schlaeger TM, Rossi DJ. Highly efficient reprogramming to pluripotency and directed differentiation of human cells with synthetic modified mRNA. *Cell Stem Cell*, **7**, 618–630 (2010).
7) Miyoshi N, Ishii H, Nagano H, Haraguchi N, Dewi DL, Kano Y, Nishikawa S, Tanemura M, Mimori K, Tanaka F, Saito T, Nishimura J, Takemasa I, Mizushima T, Ikeda M, Yamamoto H, Sekimoto M, Doki Y, Mori M. Reprogramming of mouse and human cells to pluripotency using mature microRNAs. *Cell Stem Cell*, **8**, 633–638 (2011).
8) Murry CE, Keller G. Differentiation of embryonic stem cells to clinically relevant populations: lessons from embryonic development. *Cell*, **132**, 661–680 (2008).
9) Irion S, Nostro MC, Kattman SJ, Keller GM. Directed differentiation of pluripotent stem cells: from developmental biology to therapeutic applications. *Cold Spring Harb. Symp. Quant. Biol.*, **73**, 101–110 (2008).
10) Byrne JA. Generation of isogenic pluripotent stem cells. *Hum. Mol. Genet.*, **17** (R1), R37–R41 (2008).
11) Ebert AD, Yu J, Rose FF Jr, Mattis VB, Lorson CL, Thomson JA, Svendsen CN. Induced pluripotent stem cells from a spinal muscular atrophy patient. *Nature*, **457**, 277–280 (2009).
12) Brennand KJ, Simone A, Jou J, Gelboin-Burkhart C, Tran N, Sangar S, Li Y, Mu Y, Chen G, Yu D, McCarthy S, Sebat J, Gage FH. Modelling schizophrenia using human induced pluripotent stem cells. *Nature*, **473**, 221–225 (2011).
13) Egashira T, Yuasa S, Suzuki T, Aizawa Y, Yamakawa H, Matsuhashi T, Ohno Y, Tohyama S, Okata S, Seki T, Kuroda Y, Yae K, Hashimoto H, Tanaka T, Hattori F, Sato T, Miyoshi S, Takatsuki S, Murata M, Kurokawa J, Furukawa T, Makita N, Aiba T, Shimizu W, Horie M, Kamiya K, Kodama I, Ogawa S, Fukuda K. Disease characterization using LQTS-specific induced pluripotent stem cells. *Cardiovasc. Res.*, **95**, 419–429 (2012).
14) Osafune K, Caron L, Borowiak M, Martinez RJ, Fitz-Gerald CS, Sato Y, Cowan CA, Chien KR, Melton DA. Marked differences in differentiation propensity among human embryonic stem cell lines. *Nat. Biotechnol.*, **26**, 313–315 (2008).
15) Dimos JT, Rodolfa KT, Niakan KK, Weisenthal LM, Mitsumoto H, Chung W, Croft GF, Saphier G, Leibel R, Goland R, Wichterle H, Henderson CE, Eggan K. Induced pluripotent stem cells generated from patients with ALS can be differentiated into motor neurons. *Science*, **321**, 1218–1221 (2008).
16) Hochedlinger K, Plath K. Epigenetic reprogramming and induced pluripotency. *Development*, **136**, 509–523 (2009).
17) Meissner A. Epigenetic modifications in pluripotent and differentiated cells. *Nat. Biotechnol.*, **28**, 1079–1088 (2010).
18) Tanaka T, Takahashi K, Yamane M, Tomida S, Nakamura S, Oshima K, Niwa A, Nishikomori R, Kambe N, Hara H, Mitsuyama M, Morone N, Heuser JE, Yamamoto T, Watanabe A, Sato-Otsubo A, Ogawa S, Asaka I, Heike T, Yamanaka S, Nakahata T, Saito MK. Induced pluripotent stem cells from CINCA syndrome patients as a model for dissecting somatic mosaicism and drug discovery. *Blood*, **120**, 1299–1308 (2012).
19) Goldenberg I, Moss AJ. Long QT syndrome. *J. Am. Coll. Cardiol.*, **51**, 2291–2300 (2008).
20) Marbán E. Cardiac channelopathies. *Nature*, **415**, 213–218 (2002).
21) Takahashi K, Yamanaka S. Induction of pluripotent stem cells from mouse embryonic and adult fibroblast cultures by defined factors. *Cell*, **126**, 663–676 (2006).
22) Soldner F, Hockemeyer D, Beard C, Gao Q, Bell GW, Cook EG, Hargus G, Blak A, Cooper O, Mitalipova M, Isacson O, Jaenisch R. Parkinson's disease patient-derived induced pluripotent stem cells free of viral reprogramming factors. *Cell*, **136**, 964–977 (2009).
23) Seki T, Yuasa S, Oda M, Egashira T, Yae K, Kusumoto D, Nakata H, Tohyama S, Hashimoto H, Kodaira M, Okada Y, Seimiya H, Fusaki N, Hasegawa M, Fukuda K. Generation of induced pluripotent stem cells from human terminally differentiated circulating T cells. *Cell Stem Cell*, **7**, 11–14 (2010).
24) Maherali N, Hochedlinger K. Guidelines and techniques for the generation of induced pluripotent stem cells. *Cell Stem Cell*, **3**, 595–605 (2008).
25) Gore A, Li Z, Fung H-L, Young JE, Agarwal S, Antosiewicz-Bourget J, Canto I, Giorgetti A, Israel MA, Kiskinis E, Lee JH, Loh YH, Manos PD, Montserrat N, Panopoulos AD, Ruiz S, Wilbert ML, Yu J, Kirkness EF, Izpisua Belmonte JC, Rossi DJ, Thomson JA, Eggan K, Daley GQ, Goldstein LS, Zhang K. Somatic coding mutations in human induced pluripotent stem cells. *Nature*, **471**, 63–67 (2011).
26) Laurent LC, Ulitsky I, Slavin I, Tran H, Schork A, Morey R, Lynch C, Harness JV, Lee S, Barrero MJ, Ku S, Martynova M, Semechkin R, Galat V, Gottesfeld J, Izpisua Belmonte JC, Murry C, Keirstead HS, Park HS, Schmidt U, Laslett AL, Muller FJ, Nievergelt CM, Shamir R, Loring JF. Dynamic changes in the copy number of pluripotency and cell proliferation genes in human ESCs and iPSCs during reprogramming and time in culture. *Cell Stem Cell*, **8**, 106–118 (2011).
27) Mekhoubad S, Bock C, de Boer AS, Kiskinis E, Meissner A, Eggan K. Erosion of dosage compensation impacts human iPSC disease modeling. *Cell Stem Cell*, **10**, 595–609 (2012).
28) Ohi Y, Qin H, Hong C, Blouin L, Polo JM, Guo T, Qi Z, Downey SL, Manos PD, Rossi DJ, Yu J, Hebrok M, Hochedlinger K, Costello JF, Song JS, Ramalho-Santos M. Incomplete DNA methylation underlies a transcriptional memory of somatic cells in human iPS cells. *Nat. Cell Biol.*, **13**, 541–549 (2011).
29) Soldner F, Laganière J, Cheng AW, Hockemeyer D, Gao Q, Alagappan R, Khurana V, Golbe LI, Myers RH, Lindquist S, Zhang

L, Guschin D, Fong LK, Vu BJ, Meng X, Urnov FD, Rebar EJ, Gregory PD, Zhang HS, Jaenisch R. Generation of isogenic pluripotent stem cells differing exclusively at two early onset Parkinson point mutations. *Cell*, **146**, 318–331 (2011).

30) Ananiev G, Williams EC, Li H, Chang Q. Isogenic pairs of wild type and mutant induced pluripotent stem cell (iPSC) lines from Rett syndrome patients as *in vitro* disease model. *PLoS ONE*, **6**, e25255 (2011).

31) Srivastava D. Making or breaking the heart: from lineage determination to morphogenesis. *Cell*, **126**, 1037–1048 (2006).

32) Hu B-Y, Weick JP, Yu J, Ma LX, Zhang XQ, Thomson JA, Zhang SC. Neural differentiation of human induced pluripotent stem cells follows developmental principles but with variable potency. *Proc. Natl. Acad. Sci. U.S.A.*, **107**, 4335–4340 (2010).

33) Kattman SJ, Witty AD, Gagliardi M, Dubois NC, Niapour M, Hotta A, Ellis J, Keller G. Stage-specific optimization of activin/nodal and BMP signaling promotes cardiac differentiation of mouse and human pluripotent stem cell lines. *Cell Stem Cell*, **8**, 228–240 (2011).

34) Polo JM, Liu S, Figueroa ME, Kulalert W, Eminli S, Tan KY, Apostolou E, Stadtfeld M, Li Y, Shioda T, Natesan S, Wagers AJ, Melnick A, Evans T, Hochedlinger K. Cell type of origin influences the molecular and functional properties of mouse induced pluripotent stem cells. *Nat. Biotechnol.*, **28**, 848–855 (2010).

35) Kim K, Doi A, Wen B, Ng K, Zhao R, Cahan P, Kim J, Aryee MJ, Ji H, Ehrlich LI, Yabuuchi A, Takeuchi A, Cunniff KC, Hongguang H, McKinney-Freeman S, Naveiras O, Yoon TJ, Irizarry RA, Jung N, Seita J, Hanna J, Murakami P, Jaenisch R, Weissleder R, Orkin SH, Weissman IL, Feinberg AP, Daley GQ. Epigenetic memory in induced pluripotent stem cells. *Nature*, **467**, 285–290 (2010).

36) Kim K, Zhao R, Doi A, Ng K, Unternaehrer J, Cahan P, Huo H, Loh YH, Aryee MJ, Lensch MW, Li H, Collins JJ, Feinberg AP, Daley GQ. Donor cell type can influence the epigenome and differentiation potential of human induced pluripotent stem cells. *Nat. Biotechnol.*, **29**, 1117–1119 (2011).

37) Hattori F, Chen H, Yamashita H, Tohyama S, Satoh YS, Yuasa S, Li W, Yamakawa H, Tanaka T, Onitsuka T, Shimoji K, Ohno Y, Egashira T, Kaneda R, Murata M, Hidaka K, Morisaki T, Sasaki E, Suzuki T, Sano M, Makino S, Oikawa S, Fukuda K. Nongenetic method for purifying stem cell-derived cardiomyocytes. *Nat. Methods*, **7**, 61–66 (2010).

38) Dubois NC, Craft AM, Sharma P, Elliott DA, Stanley EG, Elefanty AG, Gramolini A, Keller G. SIRPA is a specific cell-surface marker for isolating cardiomyocytes derived from human pluripotent stem cells. *Nat. Biotechnol.*, **29**, 1011–1018 (2011).

39) Nelson TJ, Martinez-Fernandez A, Terzic A. Induced pluripotent stem cells: developmental biology to regenerative medicine. *Nat. Rev. Cardiol.*, **7**, 700–710 (2010).

40) Blazeski A, Zhu R, Hunter DW, Weinberg SH, Zambidis ET, Tung L. Cardiomyocytes derived from human induced pluripotent stem cells as models for normal and diseased cardiac electrophysiology and contractility. *Prog. Biophys. Mol. Biol.*, **110**, 166–177 (2012).

41) Szabo E, Rampalli S, Risueño RM, Schnerch A, Mitchell R, Fiebig-Comyn A, Levadoux-Martin M, Bhatia M. Direct conversion of human fibroblasts to multilineage blood progenitors. *Nature*, **468**, 521–526 (2010).

42) Ambasudhan R, Talantova M, Coleman R, Yuan X, Zhu S, Lipton SA, Ding S. Direct reprogramming of adult human fibroblasts to functional neurons under defined conditions. *Cell Stem Cell*, **9**, 113–118 (2011).

43) Qiang L, Fujita R, Yamashita T, Angulo S, Rhinn H, Rhee D, Doege C, Chau L, Aubry L, Vanti WB, Moreno H, Abeliovich A. Directed conversion of Alzheimer's disease patient skin fibroblasts into functional neurons. *Cell*, **146**, 359–371 (2011).

44) Koch P, Tamboli IY, Mertens J, Wunderlich P, Ladewig J, Stüber K, Esselmann H, Wiltfang J, Brüstle O, Walter J. Presenilin-1 L166P mutant human pluripotent stem cell-derived neurons exhibit partial loss of γ-secretase activity in endogenous amyloid-β generation. *Am. J. Pathol.*, **180**, 2404–2416 (2012).

45) Nguyen HN, Byers B, Cord B, Shcheglovitov A, Byrne J, Gujar P, Kee K, Schüle B, Dolmetsch RE, Langston W, Palmer TD, Pera RR. LRRK2 mutant iPSC-derived DA neurons demonstrate increased susceptibility to oxidative stress. *Cell Stem Cell*, **8**, 267–280 (2011).

46) Itzhaki I, Maizels L, Huber I, Gepstein A, Arbel G, Caspi O, Miller L, Belhassen B, Nof E, Glikson M, Gepstein L. Modeling of catecholaminergic polymorphic ventricular tachycardia with patient-specific human-induced pluripotent stem cells. *J. Am. Coll. Cardiol.*, **60**, 990–1000 (2012).

47) Sun N, Yazawa M, Liu J, Han L, Sanchez-Freire V, Abilez OJ, Navarrete EG, Hu S, Wang L, Lee A, Pavlovic A, Lin S, Chen R, Hajjar RJ, Snyder MP, Dolmetsch RE, Butte MJ, Ashley EA, Longaker MT, Robbins RC, Wu JC. Patient-specific induced pluripotent stem cells as a model for familial dilated cardiomyopathy. *Sci. Transl. Med.*, **4**, ra47 (2012).

48) Rashid ST, Corbineau S, Hannan N, Marciniak SJ, Miranda E, Alexander G, Huang-Doran I, Griffin J, Ahrlund-Richter L, Skepper J, Semple R, Weber A, Lomas DA, Vallier L. Modeling inherited metabolic disorders of the liver using human induced pluripotent stem cells. *J. Clin. Invest.*, **120**, 3127–3136 (2010).

49) Kumano K, Arai S, Hosoi M, Taoka K, Takayama N, Otsu M, Nagae G, Ueda K, Nakazaki K, Kamikubo Y, Eto K, Aburatani H, Nakauchi H, Kurokawa M. Generation of induced pluripotent stem cells from primary chronic myelogenous leukemia patient samples. *Blood*, **119**, 6234–6242 (2012).

50) Fujikura J, Nakao K, Sone M, Noguchi M, Mori E, Naito M, Taura D, Harada-Shiba M, Kishimoto I, Watanabe A, Asaka I, Hosoda K, Nakao K. Induced pluripotent stem cells generated from diabetic patients with mitochondrial DNA A3243G mutation. *Diabetologia*, **55**, 1689–1698 (2012).

51) Shi Y, Kirwan P, Smith J, MacLean G, Orkin SH, Livesey FJ. A human stem cell model of early Alzheimer's disease pathology in Down syndrome. *Sci. Transl. Med.*, **4**, ra29 (2012).

52) Batista LFZ, Pech MF, Zhong FL, Nguyen HN, Xie KT, Zaug AJ, Crary SM, Choi J, Sebastiano V, Cherry A, Giri N, Wernig M, Alter BP, Cech TR, Savage SA, Reijo Pera RA, Artandi SE. Telomere shortening and loss of self-renewal in dyskeratosis congenita induced pluripotent stem cells. *Nature*, **474**, 399–402 (2011).

53) Agarwal S, Loh Y-H, McLoughlin EM, Huang J, Park IH, Miller JD, Huo H, Okuka M, Dos Reis RM, Loewer S, Ng HH, Keefe DL, Goldman FD, Klingelhutz AJ, Liu L, Daley GQ. Telomere elongation in induced pluripotent stem cells from dyskeratosis congenita patients. *Nature*, **464**, 292–296 (2010).

54) Jin Z-B, Okamoto S, Osakada F, Homma K, Assawachananont J, Hirami Y, Iwata T, Takahashi M. Modeling retinal degeneration using patient-specific induced pluripotent stem cells. *PLoS ONE*, **6**, e17084 (2011).

55) Mazzulli JR, Xu Y-H, Sun Y, Knight AL, McLean PJ, Caldwell GA, Sidransky E, Grabowski GA, Krainc D. Gaucher disease glucocerebrosidase and α-synuclein form a bidirectional pathogenic loop in synucleinopathies. *Cell*, **146**, 37–52 (2011).

56) Israel MA, Yuan SH, Bardy C, Reyna SM, Mu Y, Herrera C, Hefferan MP, Van Gorp S, Nazor KL, Boscolo FS, Carson CT, Laurent LC, Marsala M, Gage FH, Remes AM, Koo EH, Goldstein LS. Probing sporadic and familial Alzheimer's disease using induced pluripotent stem cells. *Nature*, **482**, 216–220 (2012).

57) Cohen JD, Babiarz JE, Abrams RM, Guo L, Kameoka S, Chiao E, Taunton J, Kolaja KL. Use of human stem cell derived cardiomyocytes to examine sunitinib mediated cardiotoxicity and electrophysiological alterations. *Toxicol. Appl. Pharmacol.*, **257**, 74–83 (2011).

58) Tanaka T, Tohyama S, Murata M, Nomura F, Kaneko T, Chen H, Hattori F, Egashira T, Seki T, Ohno Y, Koshimizu U, Yuasa